Optimization Methods for Design of Spatial Structures

Makoto Ohsaki

Department of Architecture and Architectural Engineering,
Kyotodaigaku-Katsura, Nishikyo, Kyoto 615-8540, Japan
E-mail: ohsaki@archi.kyoto-u.ac.jp,
Tel: +81-75-383-2901, Fax: +81-75-383-2972

Summary:

Optimization methods are presented for design of shells and spatial structures. The effectiveness of using optimization techniques are demonstrated by the following examples:

1. Shape design of ribbed shells.
2. Shape design of membrane structures.
3. Optimization of single-layer spatial truss against buckling.
4. Application of heuristic methods to optimization of space frames.

The readers may first see the numerical results to find what is possible by optimization. In the appendix, overview of structural optimization in architectural design is presented, and effectiveness of optimization is demonstrated by small examples.

Each chapter is a part of a published paper, or translation from a Japanese article. So there might be some difficulties for understanding the details, inconsistency of the story, etc., which the author hope not to lead to major difficulties for understanding the concepts and results.

Chapter 1

Introduction

Process of architectural design can be conceived as a kind of optimization, where architects and structural designers (engineers) try to find their best or optimal shape and design. Especially for spatial structures covering large space, optimization techniques can be effectively applied, because we have rather small restriction for determining the shape, structural type, configuration, material, etc., for designing such structures.

Furthermore, for flexible structures such as membranes and cable nets, the equilibrium analysis itself can be done through optimization. The shape of membrane has been traditionally defined by minimal surface that minimizes the area of the surface for given boundary. Also, shape of cable nets can be determined using the principle of minimum potential energy.

On the other hand, structural and shape optimization has been extensively studied and applied in the fields of mechanical engineering and aeronautical engineering. Empirical approaches to seek for mechanically optimal shapes can be traced back to Greek or Roman Era. However, the first work of structural optimization based on modern mathematics and mechanics may be shape optimization of a column by Lagrange in 18th century. After 1970s, numerous number of computational approaches have been developed for structural optimization, and now it is possible to optimize complex structures such as the shape and topology of three-dimensional mechanical parts, and airfoils considering interaction between fluid and structure.

Among many types of architectural structures, optimization techniques can be effectively applied to spatial structures where the performance of the structure greatly depends on the shape and weight that can be optimized. In the following chapters, some optimization results are presented. Chapters 2–4 are the parts of the following papers 2–4, respectively. The readers who are interested in optimization of spatial structures can consult the references listed in each chapter, and also the following website:

http://www.archi.kyoto-u.ac.jp/~ais/staff/ohsaki/index-e.html

1. M. Ohsaki, T. Ogawa and R. Tateishi, Shape optimization of curves and surfaces considering fairness metrics and elastic stiffness, Struct. Multidisc. Optim., Vol. 24, pp. 449-456, 2003, Erratum: Vol. 27, pp. 250-258, 2004.

2. M. Ohsaki and J. Fujiwara, Developability conditions for prestress optimization of a curved surface, Comp. Meth. Appl. Mech. Engng., Vol. 192, pp. 77-94, 2003.

3. M. Ohsaki, Structural optimization for specified nonlinear buckling load factor, Japan J. of Industrial and Appl. Math., Vol. 19, No. 2, pp. 163-179, 2002.

Chapter 2

Shape optimization of curves and surfaces considering fairness metrics and elastic stiffness

2.1 Introduction.

Fairness metrics have been extensively used for automatic generation of curves and for interpolation of points by a smooth curve. In the conventional approach, the square norms of curvature and variation of curvature are minimized, respectively, to obtain the *minimum energy curve* and the *minimum variation curve* [13, 14]. Subramainan and Suchithran [26] presented a method for adjusting the knot vector of a B-spline curve based on the derivative of curvature in the process of designing ship hulls. For surfaces, the principal curvatures, mean curvature, Gaussian curvature, and their derivatives can be used for formulating the fairness metrics [2, 10, 11, 25].

After fairness or smoothness is defined, an optimization technique is to be applied to obtain an optimal curve or surface that minimizes or maximizes the given fairness metric as objective function. Evaluation of the derivatives of curvatures, however, needs much computational cost especially for surfaces. Therefore, the fairness metrics involving differentiation of curvatures are not practically acceptable for large and complex structures.

In addition to the conventional fairness metrics based on the curvatures, several advanced formulations have been presented for designing smooth curves and surfaces [22, 23]. The fairness metrics are classified into roundness, rolling, flattening, etc. There have been several practical applications of those metrics to ship hull design [16]. Ohsaki and Hayashi [18] presented a modified version of the roundness metric by Rando and Rourier for optimizing ribbed shells. It has been pointed out, however, that the fairness metrics by Rando and Rourier do not always conform to the human impressions [9, 18].

In most of the surface design methods, the surfaces are divided into several regions, each of which is defined by a parametric surface such as Bézier patch and B-spline patch. In this case, constraints should be given for continuity and intersection between the adjacent regions [2, 6]. Boundary conditions should also be given to formulate a constrained optimization problem [17, 27]. The formulations for continuity in curvatures of surfaces, however, are very complicated, and it is inconvenient that the constraints should be modified and optimization problem itself should be reformulated depending on the types of the desired surfaces; e.g., sometimes discontinuity is allowed between the tangent vectors in the adjacent regions.

Optimization of curved structures such as arches and shells under mechanical constraints is called shape optimization which has been extensively studied in the literature [24]. However, shape and topology optimization based on the ground structure approach with fixed nodal locations of the

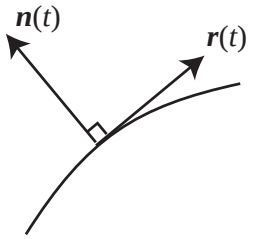

Fig. 2.1: Unit tangent and normal vectors.

Fig. 2.2: Double circular arches with same curvature.

finite element model is out of scope of the present paper. We only consider optimization of curves and surfaces that represent arches and thin shells. Parametric surfaces such as Bézier surfaces and B-spline surfaces are very useful for generating a smooth surface within small number of design variables. Ramm [20] optimized a shell defined by the Bézier surface considering stress deviation or fundamental frequency. The method has been extended to the problem with buckling constraints [21] and optimization of membrane fabric structures [3]. Ohsaki `et al.` [19] presented a trade-off design method between smoothness and elastic stiffness of an arch-type truss. Kegl and Antes [12] optimized a single-layer truss under constraints on stresses considering geometrical nonlinearity. Ohsaki and Hayashi [18] presented a method for generating round ribbed shells. In their method, however, the number of ribs should be defined in advance, and the shell should be modeled by different number of Bézier surfaces depending on the number of ribs. It is not convenient that the problem formulation depends on the desired optimal shape.

In this paper, a method is presented for generating round curves and surfaces allowing discontinuities in tangent vectors and curvatures. The distance of the center of curvature from the specified point is used for formulating the objective function which is a continuous function of the design variables through convex and concave shapes. Since the derivatives of curvatures are not used, a ribbed shell can be generated without any trouble by specifying the center of curvature of the surface or the isoparametric curves. Optimal shapes are also found under constraints on compliance that is regarded as a mechanical performance measure. A multiobjective optimization problem is solved by the constraint approach to generate a trade-off design between roundness and mechanical performance.

2.2 Shape optimization of plane curves.

2.2.1 Problem formulation.

Let $\mathbf{x}(t)$ denote a plane curve defined by a parameter $t \in [0, 1]$. The fundamentals on geometry of curves may be referred to; e.g., [5, 8]. Let $\mathbf{r}(t)$ denote the unit tangent vector of $\mathbf{x}(t)$. The unit normal vector $\mathbf{n}(t)$ is defined as shown in Fig. 2.1 by rotating $\mathbf{r}(t)$ by $\pi/2$. The curvature of $\mathbf{x}(t)$ is denoted by $\kappa(t)$. The curvature of the curve shown in Fig. 2.1 has negative values, because the center of curvature exists in the opposite direction of $\mathbf{n}(t)$ from a point along the curve.

The curvature is an intrinsic property of a curve that does not depend on parameterization. Therefore, the fairness of a curve can be controlled through $\kappa(t)$. In this section, we present an optimization method for generating round curves for the given span length. A simple approach may be to specify the desired value $\bar{\kappa}$ of $\kappa(t)$ and minimize the norm of deviation $(\kappa(t) - \bar{\kappa})^2$. Moreton and Séquin [15] noted, however, that a metric defined simply by $\kappa(t)$ or its derivative with respect to t is scale variant; i.e., it depends on the size of the curve, and the tangent vectors should be given at the boundaries to obtain a desired shape by using such a metric.

For a single arch spanning two supports, the *fundamental theorem of the local theory of curves* guarantees that the arch is uniquely determined by specifying $\kappa(t)$ [5]. For double arches as shown in

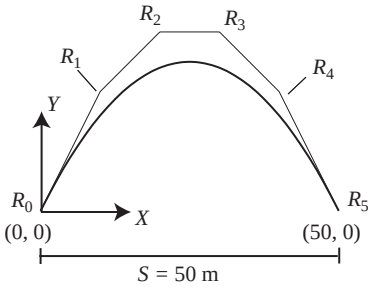

Fig. 2.3: Initial curve (a)

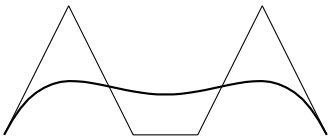

Fig. 2.4: Initial curve (b)

Fig. 2.2, they cannot be uniquely determined from $\kappa(t)$; i.e., the tangent vectors at two ends should be given. It is inconvenient, however, to specify tangent vectors especially if extended to surfaces. Therefore, we use the center of curvature for generating round curves and surfaces without assigning tangent vectors.

In a standard approach to generating a double arch as shown in Fig. 2.2, the total curve is divided into two regions, each of which is defined by a parametric curve. In this case, however, the problem formulation depends on the number of regions. If a sufficiently large number of regions are given, then constraints should be assigned for continuity between the adjacent regions to generate an optimal curve with smaller number of arches. The number of variables becomes unnecessarily large and the continuity conditions for curvatures are very complicated for surface optimization. Therefore, we present a unified approach by using a single Bézier curve to generating optimal curves with different numbers of arches.

The center of curvature $\mathbf{c}(t)$ is defined for $\kappa(t) \neq 0$ as

$$\mathbf{c}(t) = \mathbf{x}(t) + \frac{1}{\kappa(t)}\mathbf{n}(t) \tag{2.1}$$

The curve $\mathbf{x}(t)$ is defined as follows by the Bézier curve of order n [7]:

$$\mathbf{x}(t) = \sum_{i=0}^{n} \mathbf{R}_i B_i^n(t) \tag{2.2}$$

where $\mathbf{R}_i = (R_i^x, R_i^y)$ and $B_i^n(t)$ $(i = 0, \ldots, n)$ are the control points and the Bernstein polynomials of order n, respectively.

In the following examples, $n = 5$ and the control polygon is as illustrated in thin lines in Fig. 2.3. The (X, Y)-coordinates are also defined as shown in Fig. 2.3. Optimal shapes are found from two different initial curves (a) and (b) as shown in Figs. 2.3 and 2.4, respectively, where curve (a) has negative curvature, and curve (b) has regions with positive and negative curvatures. Based on the symmetry property, the curve is defined by $\mathbf{R}_0$, $\mathbf{R}_1$ and $\mathbf{R}_2$. The vector consisting of all the variables is denoted by $\mathbf{R}$.

Let $\mathbf{c}_0$ denote the specified center of curvature. Differentiation with respect to t is indicated by a dot. The length of the tangent vector $\dot{\mathbf{x}}(t)$ is denoted by $g(t)$; i.e., $\mathrm{d}s = g(t)\mathrm{d}t$ for the arc-length parameter s. Let $(\,\cdot\,; \mathbf{R})$ indicate a function that depends on $\mathbf{R}$. The square of distance between $\mathbf{c}(t; \mathbf{R})$ and $\mathbf{c}_0$ is defined as

$$d(t; \mathbf{R}) = ||\mathbf{c}(t; \mathbf{R}) - \mathbf{c}_0||^2 \tag{2.3}$$

where $||\cdot||$ is the Euclidean norm of a vector. The optimization problem may be simply formulated as

$$\text{P1:} \quad \text{Minimize} \int_0^1 d(t; \mathbf{R}) g(t; \mathbf{R}) \mathrm{d}t \tag{2.4}$$

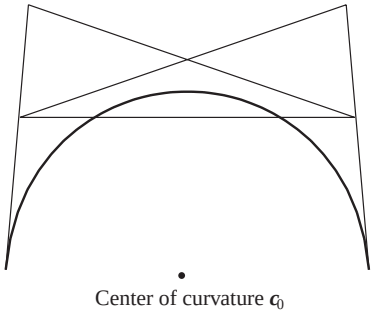

Fig. 2.5: Optimal curve for $\mathbf{c}_0 = (25, 0)$.

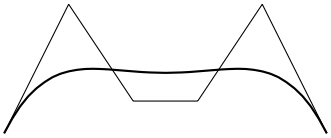

Fig. 2.6: Intermediate curve during optimization.

An optimal shape as illustrated in Fig. 2.5 can be obtained by solving P1 from the initial curve (a). Details of the mathematical formulations will be shown in the examples. From the initial curve (b), however, the curve in Fig. 2.5 has to be reached through an intermediate curve as illustrated in Fig. 2.6 of which the center of curvature around the center $t = 0.5$ is far from $\mathbf{c}_0$ and even in the opposite side of the curve. Therefore, the optimal solution of Fig. 2.5 cannot be obtained by solving P1 from the initial curve (b).

Let T denote the region of t where $\kappa(t) < 0$ is satisfied. It is possible that the integration of (2.4) is to be done only over the region T. In this case, however, there is no region for integration if $\kappa(t) > 0$ is satisfied throughout the region. Therefore, a curve with positive curvature in $t \in [0, 1]$ is obtained from the initial curve (b) because P1 is a minimization problem with nonnegative objective function and a solution with $\kappa(t) > 0$ throughout the region has vanishing objective value that leads to an obvious and meaningless optimal solution. The problem may alternatively be written as

$$\text{P2:}\quad \text{Maximize} \int_{t\in T} \frac{1}{d(t;\mathbf{R})} g(t;\mathbf{R})\mathrm{d}t \tag{2.5}$$

In the process of solving P2, the design variables are to be modified so that $d(t;\mathbf{R})$ is reduced and $\kappa(t) < 0$ is to be satisfied in wider region of t. Therefore, as shown in the following examples, the optimal curve in Fig. 2.5 is successfully obtained from the initial curve (b). Note that the objective function diverges if $d(t;\mathbf{R}) = 0$ is satisfied at a point. In order to prevent the divergence, the value of $1/d(t;\mathbf{R})$ is replaced by $\bar{d}$ if $1/d(t;\mathbf{R}) > \bar{d}$, and P2 is reformulated as

$$\text{P3:}\quad \text{Maximize} \int_{t\in T} \min\left\{\frac{1}{d(t;\mathbf{R})}, \bar{d}\right\} g(t;\mathbf{R})\mathrm{d}t \tag{2.6}$$

In numerical implementation, the parameter region is divided uniformly by the interval Δt, and the value of t at the center of the ith region is denoted by t_i. Upper and lower bounds for $\mathbf{R}$ are given as $\mathbf{R}^U$ and $\mathbf{R}^L$, respectively. Finally, the optimization problem to be solved is formulated as

$$\text{P4:}\quad \text{Maximize} \quad \sum_{t_i\in T} \min\left\{\frac{1}{d(t;\mathbf{R})}, \bar{d}\right\} g(t_i;\mathbf{R})\Delta t \tag{2.7}$$

$$\text{subject to:}\quad \mathbf{R}^L \le \mathbf{R} \le \mathbf{R}^U \tag{2.8}$$

$$\mathbf{H}(\mathbf{R}) \le \mathbf{0} \tag{2.9}$$

where $\mathbf{H}(\mathbf{R}) \le \mathbf{0}$ denotes the geometrical constraints given if necessary. The variations of the objective values of P1 and P4 between the initial and the optimal solutions are compared in the examples.

A round shape is generated by solving P4. The mechanically optimal shape, however, is quite different from a round shape. Therefore, we next consider the trade-off between roundness and

mechanical property defined by compliance (external work) against static loads. The arch is divided into regions with equal parameter length which are modeled by standard beam elements. Let $\mathbf{F}$ and $\mathbf{U}$ denote, respectively, the vectors of nodal loads and nodal displacements obtained by solving

$$\mathbf{KU} = \mathbf{F} \tag{2.10}$$

where $\mathbf{K}$ is the linear elastic stiffness matrix, and dependence of all the variables on $\mathbf{R}$ is assumed. The compliance W is defined by $\mathbf{F}^T\mathbf{U}$. The specified structural volume is denoted by $\bar{V}$. The cross-sectional area A is then given by $A = \bar{V}/L$ where L is the total length of the arch. The optimization problem is formulated as

$$\begin{aligned} \text{P5:}\quad \text{Minimize} \quad & W(\mathbf{R}) && (2.11)\\ \text{subject to:} \quad & \mathbf{R}^L \le \mathbf{R} \le \mathbf{R}^U && (2.12)\\ & \mathbf{H}(\mathbf{R}) \le \mathbf{0} && (2.13) \end{aligned}$$

Since the roundness and the elastic stiffness defined by using the compliance can be conceived as conflicting performance measures, a multiobjective optimization problem can be formulated for optimizing the two objectives [4]. There are many approaches to obtaining all the possible Pareto optimal solutions or to selecting the most preferred solution among the set of Pareto optimal solutions. In this paper, a so called constraint method is used [4]. Let $\bar{W}$ denote the specified upper bound for W, and consider the following problem:

$$\begin{aligned} \text{P6:}\quad \text{Maximize} \quad & \sum_{t_i \in T} \min\left\{\frac{1}{d(t;\mathbf{R})}, \bar{d}\right\} g(t_i;\mathbf{R})\Delta t && (2.14)\\ \text{subject to:} \quad & W(\mathbf{R}) \le \bar{W} && (2.15)\\ & \mathbf{R}^L \le \mathbf{R} \le \mathbf{R}^U && (2.16)\\ & \mathbf{H}(\mathbf{R}) \le \mathbf{0} && (2.17) \end{aligned}$$

Note that $\bar{W}$ is given in view of the values of W of the optimal solutions of P4 and P5. A set of Pareto optimal solutions can be generated by solving P6 for various values of $\bar{W}$.

2.2.2 Examples of curve optimization.

Optimal curves are found from the initial shapes (a) and (b), where the span length S is 50 m. The curve is symmetric with respect to the line defined by $Y = 25$ m. The (X, Y)-coordinates of the supports, which are fixed during optimization, are defined as shown in Fig. 2.3. In the following, the unit of the length is m, which is omitted for brevity. The coordinates of $\mathbf{R}_0$, $\mathbf{R}_1$, $\mathbf{R}_2$ are $(0, 0)$, $(10, 20)$, $(20, 30)$, respectively, for initial curve (a), and $(0, 0)$, $(10, 20)$, $(20, 0)$ for initial curve (b). The variables are (X, Y)-coordinates of $\mathbf{R}_1$ and $\mathbf{R}_2$, and the number of variables is four. The upper and lower bounds are 50 and -10, respectively, for the X-coordinates, and 50 and -20 for the Y-coordinates. Optimization is carried out by IDESIGN 3.5 [1], and the sequential quadratic programming method is used.

A constraint is given such that the X-component of the tangent vector $\dot{\mathbf{x}}(t)$ is nonnegative at the center $t = 0.5$. The constraint is explicitly written as

$$R_0^x + 3R_1^x + 2R_2^x \le 3S \tag{2.18}$$

Note that Y-component of $\dot{\mathbf{x}}(t)$ vanishes at $t = 0.5$ due to the symmetry condition. Therefore, $||\dot{\mathbf{x}}(t)|| = 0$ and a cusp can exist at the center if (2.18) is satisfied in equality.

The optimal shape in Fig. 2.5 has been successfully found from the initial curve (b) by solving P4 with $\mathbf{c}_0 = (25, 0)$, where $\bar{d} = 1.0$ and $\Delta t = 0.01$. It may be observed from this result that the

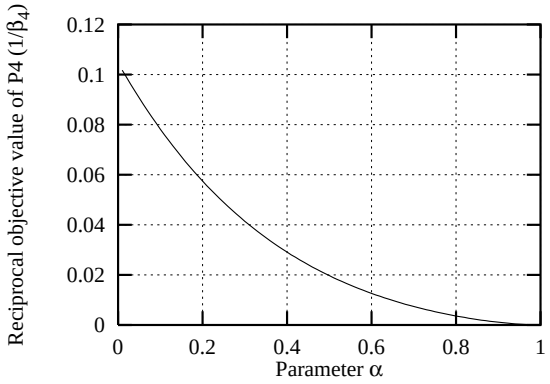

Fig. 2.7: Variation of the reciprocal objective value of P4 with respect to α.

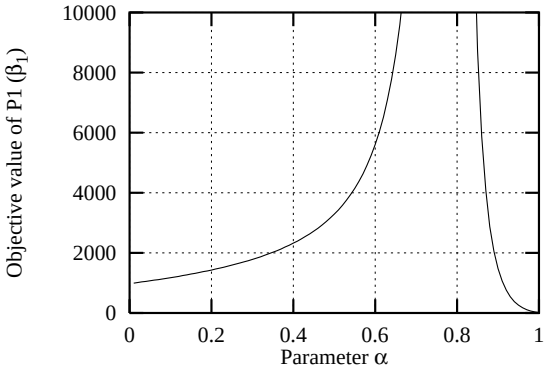

Fig. 2.8: Variation of the objective value of P1 with respect to α.

optimal shape with $\kappa(t) < 0$ throughout the region can be found from an initial solution with convex and concave regions.

Let $\mathbf{R}^{\mathrm{I}}$ and $\tilde{\mathbf{R}}$ denote the control points corresponding to the initial curve (b) and the optimal curve, respectively. In order to discuss the efficiency of using the formulation of P4, the intermediate solutions $\hat{\mathbf{R}}$ between $\mathbf{R}^{\mathrm{I}}$ and $\tilde{\mathbf{R}}$ are linearly defined by a parameter α as

$$\hat{\mathbf{R}} = \alpha\tilde{\mathbf{R}} + (1-\alpha)\mathbf{R}^{\mathrm{I}} \tag{2.19}$$

Let β_1 and β_4 denote, respectively, the objective functions of P1 and P4. Variation of $1/\beta_4$ with respect to α is plotted in Fig. 2.7. It is seen from Fig. 2.7 that $1/\beta_4$ decreases; i.e. β_4 increases; as the curve approaches the optimal curve. Therefore, the optimal solution can be obtained by solving P4. On the contrary, β_1 is a discontinuous function of α as shown in Fig. 2.8. Although the objective value has the minimum value at $\alpha = 1$, it is very difficult to reach the optimal solution from the initial solution (b).

If $\mathbf{c}_0 = (12.5, 0)$ is given for the left side with $0 \le t \le 0.5$, the optimal curve as shown in Fig. 2.9 has been reached from the initial curve (a). It may be observed from these results that optimal solutions with various types of curvature distributions can be obtained by specifying the center of curvature, and curves with single and double arches can be obtained without any modification of problem formulation or geometrical modeling.

Next, we consider compliance as a mechanical performance measure. The material is steel where the elastic modulus E is 200.0 GPa and the weight density is 80.0 kN/m^3. The cross-section of the arch is sandwich, and the distance between the two flanges is denoted by h. In this case, the extensional stiffness is EA and the bending stiffness is $EAh^2/4$, where $h = 1$ m in the following. The arch has pin supports, and is divided into 20 beam elements. Distributed load of 2.0 kN per unit arc-length is applied in the negative Y-direction in addition to the self weight. The specified total structural volume $\bar{V}$ is 20.0 m^3. The optimal solution for minimizing W is as shown in Fig. 2.10, where the optimal value of W is 9.3117×10^2 kNm.

It is observed from Figs. 2.5 and 2.10 that the optimal shape for minimizing the compliance is quite different from the round shape. The values of W for the optimal round curves in Figs. 2.5 and 2.9 are 7.5503×10^3 kNm and 9.8876×10^4 kNm, respectively. Problem P6 has been next solved with $\mathbf{c}_0 = (25.0, 0)$ and $\bar{W} = 1.0 \times 10^3$ kNm. Fig. 2.11 shows the obtained optimal shape. It is seen from Fig. 2.11 that an intermediate solution between Figs. 2.5 and 2.10 has been obtained by considering the trade-off between roundness and elastic stiffness.

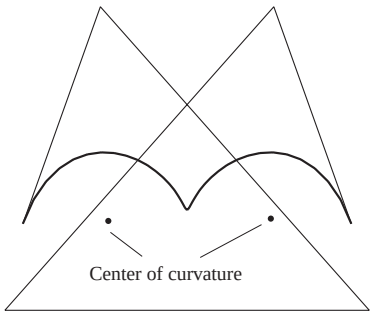

Fig. 2.9: Optimal shape for $\mathbf{c}_0 = (12.5, 0)$.

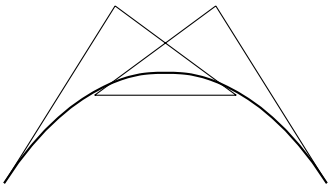

Fig. 2.10: Optimal solution for minimizing compliance ($W = 7.5503 \times 10^3$ kNm).

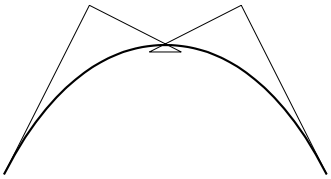

Fig. 2.11: Optimal solution for $\mathbf{c}_0 = (25, 0)$ under constraint on compliance ($W = 1.0 \times 10^4$ kNm).

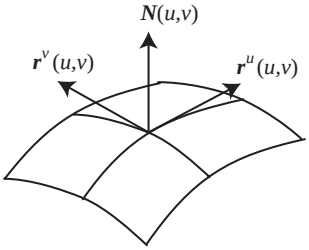

Fig. 2.12: Unit tangent and normal vectors of a surface.

2.3 Shape optimization of surfaces.

2.3.1 Problem formulation.

Consider a surface defined by parameters u and v as $\mathbf{X}(u, v)$. The fundamentals on geometry of surfaces may be referred to; e.g., [5, 8]. We use curvatures and unit normal vectors also for optimization of surfaces. The unit normal vector of the surface is denoted by $\mathbf{N}(u, v)$. A line in u- or v-direction in the parameter space corresponds to a curve in the physical space which is called an *isoparametric curve*. Let $\mathbf{r}^u(u, v)$ and $\mathbf{r}^v(u, v)$ denote the unit tangent vectors of the isoparametric curves in u- and v-directions, respectively. $\mathbf{N}(u, v) = \mathbf{r}^u(u, v) \times \mathbf{r}^v(u, v)$ is defined as shown in Fig. 2.12.

Let $\kappa_i(u, v)$ $(i = 1, 2)$ denote the two principal curvatures at a point on a surface. The centers of curvatures can be defined as

$$\mathbf{P}_i(u, v) = \mathbf{X}(u, v) + \frac{1}{\kappa_i(u, v)}\mathbf{N}(u, v), \quad (i = 1, 2) \tag{2.20}$$

The formulation (2.20), however, can not be conveniently used for specifying the desired shape, because two centers of curvatures exist at a point on the surface.

If the Gaussian curvature $K(u, v) = \kappa_1(u, v)\kappa_2(u, v)$ is used, the center of curvature can be uniquely determined as follows for $K(u, v) > 0$ [11]:

$$\mathbf{C}(u, v) = \mathbf{X}(u, v) + \frac{1}{\sqrt{K(u, v)}}\mathbf{N}(u, v) \tag{2.21}$$

Note that the surface of Fig. 2.12 has two negative principal curvatures and $K(u, v) > 0$.

The surface $\mathbf{X}(u, v)$ is defined by the tensor product Bézier surface as [7]

$$\mathbf{X}(u, v) = \sum_{i=0}^{n}\sum_{j=0}^{m}\mathbf{R}_{i,j}B_i^n(u)B_j^m(v) \tag{2.22}$$

where $\mathbf{R}_{i,j} = (R^x_{i,j}, R^y_{i,j})$ $(i = 0, \ldots, n; j = 0, \ldots, m)$ are the control points, and $n = m = 5$ in the following examples.

Let $\mathbf{C}_0$ denote the specified center of curvature for the definition (2.21). The parameters u and v $\in [0, 1]$ are divided into regions with uniform interval by Δu and Δv, respectively, and the parameter values at the centers of the regions are denoted by u_i and v_j. The determinant of the first fundamental matrix of the surface is denoted by $G(u, v)$. Note that $\mathbf{N}(u, v)$ defined in Fig. 2.12 is in the same direction irrespective of the sign of the principal curvatures. Let U denote the region where both of the principal curvatures are negative. The square of distance between $\mathbf{C}(u_i, v_j; \mathbf{R})$ and $\mathbf{C}_0$ is defined as

$$D(u_i, v_j; \mathbf{R}) = ||\mathbf{C}(u_i, v_j; \mathbf{R}) - \mathbf{C}_0||^2 \tag{2.23}$$

The optimization problem for specified center of curvature is formulated as

$$\begin{aligned} \text{P7: Maximize} \quad & \sum_{(u_i, v_j) \in U} \min \left\{ \frac{1}{D(u_i, v_j; \mathbf{R})}, \bar{d} \right\} \\ & \times \sqrt{G(u_i, v_j; \mathbf{R})} \Delta u \Delta v \qquad (2.24) \\ \text{subject to:} \quad & \mathbf{R}^L \leq \mathbf{R} \leq \mathbf{R}^U \qquad (2.25) \\ & \mathbf{H}(\mathbf{R}) \leq \mathbf{0} \qquad (2.26) \end{aligned}$$

A round surface is obtained by solving P7.

The center of curvature can alternatively be defined by the isoparametric curves for generating a ribbed shell. Let $\kappa^u(u; v)$ denote the curvature of the isoparametric curve in u-direction, where the argument $(u; v)$ indicates that the parameter is u, but the curve is defined for each specified value of v. The unit normal vector is denoted by $\mathbf{n}^u(u; v)$. Note that $\kappa^u(u; v)$ of a curve in three dimensional space always has nonnegative value. The center of curvature of the isoparametric curve is given for the region $\kappa^u(u; v) \neq 0$ as

$$\mathbf{c}^u(u; v) = \mathbf{X}(u, v) + \frac{1}{\kappa^u(u; v)} \mathbf{n}^u(u; v) \tag{2.27}$$

$\mathbf{c}^v(u; v)$ can be defined similarly.

2.3.2 Examples of surface optimization.

Optimal shapes have been found from the initial shapes (a) and (b) as shown in Figs. 2.13 and 2.14, respectively. We only consider the surfaces that are symmetric with respect to the planes defined by $X = 25$ and $Y = 25$. The (X, Y, Z)-coordinates are defined as shown in Fig. 2.13. Based on the symmetry conditions, the surface is defined by nine control points $\mathbf{R}_{i,j}$, $(i = 0, 1, 2; j = 0, 1, 2)$. For the initial shape (a), $\mathbf{R}_{0,0} = (0, 0, 0)$, $\mathbf{R}_{0,1} = (0, 10, 0)$, $\mathbf{R}_{0,2} = (0, 20, 0)$, $\mathbf{R}_{1,0} = (10, 0, 0)$, $\mathbf{R}_{1,1} = (10, 10, 20)$, $\mathbf{R}_{1,2} = (10, 20, 20)$, $\mathbf{R}_{2,0} = (20, 0, 0)$, $\mathbf{R}_{2,1} = (20, 10, 20)$, $\mathbf{R}_{2,2} = (20, 20, 20)$. For the initial shape (b), $\mathbf{R}_{2,2} = (20, 20, -10)$ and the remaining control points are same as those of (a). The control polygons are plotted in thin lines in Figs. 2.13 and 2.14.

The three components of $\mathbf{R}_{0,0}$ are fixed during the optimization process. The control points along the boundary can move only in the vertical planes in which the boundary curves are located. The upper and lower bounds are 50 and 0, respectively, for X, Y-coordinates, and 60 and -20 for Z-coordinates. The parameters are divided by $\Delta u = \Delta v = 0.0125$. The upper bound $\bar{d}$ in (2.24) is 1.0. Geometrical constraints are given so that the X- and Y-components of the tangent vectors of the isoparametric curves in u- and v-directions, respectively, have nonnegative values at the points on

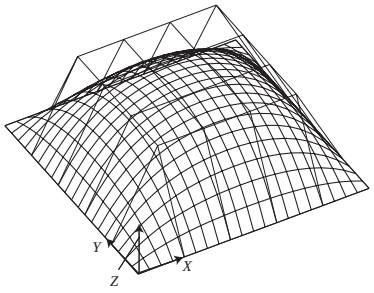

Fig. 2.13: Initial solution (a).

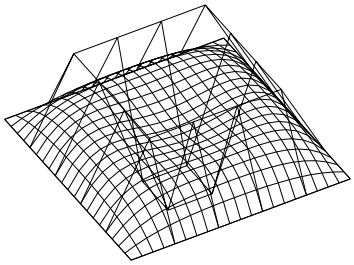

Fig. 2.14: Initial solution (b).

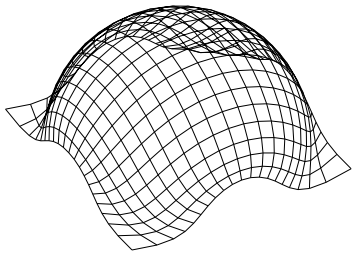

Fig. 2.15: Optimal solution for $\mathbf{C}_0 = (25, 25, 0)$.

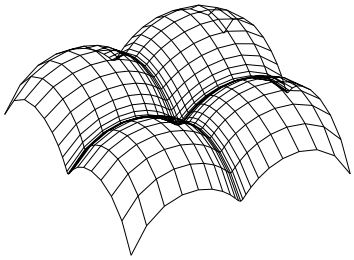

Fig. 2.16: Optimal solution for $\mathbf{C}_0 = (12.5, 12.5, 0)$.

the planes of symmetry defined by $u = 0.5$ and $v = 0.5$. These constraints are then written explicitly as

$$R^x_{0,j} + 3R^x_{1,j} + 2R^x_{2,j} \leq 3S^x, \quad (j = 0, 1, 2) \tag{2.28}$$

$$R^x_{i,0} + 3R^x_{i,1} + 2R^x_{i,2} \leq 3S^y, \quad (i = 0, 1, 2) \tag{2.29}$$

where S^x and S^y are the span lengths in X- and Y-directions, respectively, which are equal to 50.0 m.

The optimal solution for $\mathbf{C}_0 = (25, 25, 0)$ is as shown in Fig. 2.15 which has been obtained from the initial solution (b) as shown in Fig. 2.14. A round surface has been successfully reached from a partially concave initial shape. Note that there exist concave regions at four corners. Roundness in almost all the domain, however, has been increased by sacrificing smoothness at the corners of the optimal shape.

An optimal shape of Fig. 2.16 has been found for $\mathbf{C}_0 = (12.5, 12.5, 0)$ from the initial shape (a); i.e., a ribbed shell with discontinuity in the tangent vector can be found from a convex initial shape. Therefore, optimal shape with various curvature distributions can be generated by solving P7 from different types of initial shapes.

Consider next a problem of minimizing the compliance under static loads. The curved shell is assumed to be sufficiently thin so that only membrane stresses should be considered. The standard nine-degree-of-freedom triangular element with uniform stresses and strains is used [28]. The parameter space (u, v) is divided into 20×20 regions with same interval. The shell is subjected to distributed load 100.0 N in negative Z-direction per unit area of the surface. The material is steel, and all the displacement components including rotations are fixed along the boundary. The specified structural volume is 10.0 m^3.

The optimal solution is as shown in Fig. 2.17, where the compliance is 5.6934×10^3 kNm. It is seen from Fig. 2.17 that the optimal shell has a kind of cylindrical shell with parabolic cross-section in each direction of X and Y. The value of W for the shells in Figs. 2.15 and 2.16 are 6.2064×10^4 kNm and 5.9848×10^4 kNm, respectively. The trade-off solution for $\mathbf{C}_0 = (25, 25, 0)$ and $\bar{W} = 7.0 \times 10^3$

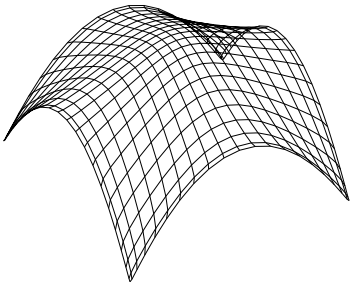

Fig. 2.17: Optimal shape for minimizing compliance ($W = 5.6934 \times 10^3$ kNm).

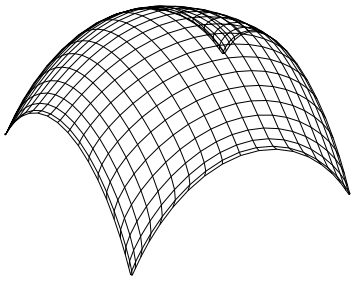

Fig. 2.18: Optimal shape under compliance constraint ($W = 7.0 \times 10^3$ kNm).

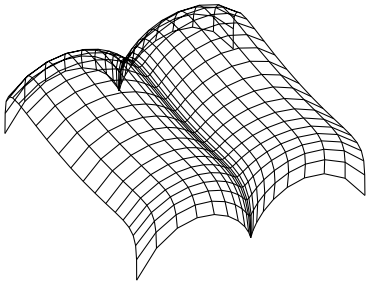

Fig. 2.19: Optimal shape for specified center of curvature of isoparametric curve.

kNm is as shown in Fig. 2.18 which is between the shapes in Figs. 2.15 and 2.17.

Finally, a ribbed shell is generated by using the center of curvature of the isoparametric curve given by (2.27). The inverse of the square of the distance between $\mathbf{c}^u(u;v)$ and the line defined by $X = 12.5, Z = 0$ for the region $u \in [0, 0.5]$ and $v \in [0, 1]$ has been minimized to obtain the optimal shape in Fig. 2.19, where $\bar{d} = 1.0$ has also been used, and the integration has been carried out only for the region with $\kappa^u(u;v) < 0$. It is observed from Fig. 2.19 that a ribbed shell can be generated by specifying the center of curvature of the isoparametric curve without any modification of modeling method of the surface.

2.4 Conclusions.

A unified approach has been presented for generating round shells with and without ribs from initial shapes with various distributions of curvature. The conclusions drawn from this study are summarized as follows:

1. A smooth convergence of the objective function to the optimal objective value has been demonstrated in the example of a curve optimization by using the objective function defined by the inverse of distance of the center of curvature from the specified point, where the region of the integration of the objective function is restricted by the signs of principal curvatures.

2. Dependence of the optimization result on the initial shape can be successfully avoided by using the proposed formulation, and round curves and surfaces with different numbers of arches and ribs can be generated by specifying the center of curvature without any modification of problem formulation or modeling method.

3. The shape of a ribbed shell or a double arch cannot uniquely be defined only by the curvature distribution and the boundary conditions.

4. The optimal shape for minimizing compliance under constraint on structural volume has been shown to be a doubly curved shell that consists of cylindrical shell in two directions.

5. The constraint approach can be successfully used for obtaining a trade-off design between round and mechanically efficient shapes.

6. A ribbed cylindrical shell can be generated by specifying the distribution of the center of curvature of the isoparametric curves.

It may be observed from these results that the center of curvature is an intrinsic property that directly corresponds to the shape of the curves and surfaces, and various round shapes with and without ribs can be generated by specifying the center of curvatures within a unified problem formulation.

References

[1] Arora, J. and Tseng, C. (1987). Idesign user's manual, ver. 3.5. Technical report, Optimal Design Laboratory, The University of Iowa.

[2] Barnhill, R. E., editor (1994). *Geometry Processing for Design and Manufacturing*. SIAM.

[3] Bletzinger, K.-U. (1999). Structural optimization and form finding of lightweight structures. In *Proc. 3rd World Congress of Structural and Multidisciplinary Optimization (WCSMO3)*.

[4] Cohon, J. L. (1978). *Multiobjective Programming and Planning*, volume 140 of *Mathematics in Science and Engineering*. Academic Press.

[5] do Carmo, M. P. (1976). *Differential Geometry of Curves and Surfaces*. Prentice-Hall.

[6] Du, W.-H. and Schmitt, F. J. M. (1990). On the g^1 continuity of piecewise Bézier surfaces: a review with new results. *Comput. Aided Des.*, **22**(9), 556–573.

[7] Farin, G. (1992). *Curves and Surfaces for Computer Aided Geometric Design*. Academic Press.

[8] Faux, I. D. and Pratt, M. J. (1979). *Computational Geometry for Design and Manufacture*. Ellis Horwood.

[9] Gerostathis, T. P., Koras, G. D., and Kaklis, P. D. (1999). Numerical experimentation with the Roulier-Rando fairness metrics. *Mathematical Engineering in Industry*, **7**(2), 195–210.

[10] Greiner, G. (1994). Variational design and fairing of spline surfaces. *Computer Graphics Forum*, **13**(3), 143–154.

[11] Hangen, H., Hahmann, S., and Schreiber, T. (1995). Visualization and computation of curvature behaviour of freeform curves and surfaces. *Comput. Aided Des.*, **27**(7), 545–552.

[12] Kegl, M. and Antes, H. (1998). Shape optimal design of elastic space frames with non-linear response. *Int. J. Num. Meth. Engng.*, **43**, 93–110.

[13] Meier, H. and Nowacki, H. (1987). Interpolating curves with gradual changes in curvature. *Comput. Aided Geom. Des.*, **4**, 297–305.

[14] Moreton, H. P. and Séquin, C. H. (1992). Functional optimization for fair surface design. *Computer Graphics*, **26**(2), 167–176.

[15] Moreton, H. P. and Séquin, C. H. (1993). Scale-invariant minimum-cost curves: Fair and robust design implements. *Computer Graphics Forum*, **12**(3), 473–484.

[16] Nowacki, H. and Reese, D. (1983). Design and fairing of ship surfaces. In R. E. Barnhill and W. Bohem, editors, *Surfaces in CAGD*, pages 121–134. North-Holland.

[17] Nowacki, H., Liu, D., and LÜ, X. (1990). Fairing Bézier curves with constraints. *Comput. Aided Geom. Des.*, **7**, 43–55.

[18] Ohsaki, M. and Hayashi, M. (2000). Fairness metrics for shape optimization of ribbed shells. *J. Int. Assoc. Shells and Spatial Struct.*, **41**(1), 31–39.

[19] Ohsaki, M., Nakamura, T., and Isshiki, Y. (1998). Shape-size optimization of plane trusses with designer's preference. *J. Struct. Engng., ASCE*, **124**(11), 1323–1330.

[20] Ramm, E. (1992). Shape finding methods of shells. *Bulletin of Int. Assoc. for Shell and Spatial Struct*, **33**(2), 89–98.

[21] Ramm, E., Bletzinger, K.-U., and Reitinger, R. (1993). Shape optimization of shell structures. *Bulletin of Int. Assoc. for Shell and Spatial Struct*, **34**(2), 103–121.

[22] Rando, T. and Roulier, J. A. (1991). Designing faired parametric surfaces. *Comput. Aided Des.*, **23**, 492–497.

[23] Roulier, J. and Rando, T. (1994). Measures of fairness for curves and surfaces. In N. S. Spadis, editor, *Designing Fair Curves and Surfaces*, pages 75–122. SIAM.

[24] Rozvany, G. I. N., editor (1992). *Shape and Layout Optimization of Structural Systems and Optimality Criteria Methods*. Springer.

[25] Sarraga, R. F. (1998). Recent methods for surface shape optimization. *Comput. Aided Geom. Des.*, **15**, 417–436.

[26] Subramainan, V. A. and Suchithran, P. R. (1999). Interactive curve fairing and bi-quintic surface generation for ship design. *Int. Shipbuild. Progr.*, **46**(446), 189–208.

[27] Welch, W. and Witkin, A. (1992). Variational surface modeling. *Computer Graphics*, **26**(2), 157–166.

[28] Zienkiewicz, O. C. and Taylor, R. L. (1989). *The Finite Element Method*. McGraw-Hill.

Chapter 3

Developability Conditions for Prestress Optimization of a Curved Surface

3.1 Introduction.

Curved surfaces in engineering fields such as membrane fabric structures are made by stretching and connecting pieces of plane sheets. Prestresses are given so that the surface retains stability and stiffness against external loads. One of the main difficulties in designing the membrane structures is that the shape of self-equilibrium is to be formed only by membrane (in-plane) stresses, because the flexural stiffness of the fabric is negligibly small. Another difficulty is that the curved surface should be formed from plane sheets by stretching only the boundaries of the sheets. In the traditional methods of designing membrane structures, an equilibrium surface is first found without considering the conditions for the surface to be reduced to plane sheets by removing the prestresses [1–5]. This process is called form-finding analysis. After equilibrium shape and prestresses are determined, the approximate plane sheets are obtained by cutting the surface along the geodesic lines, and by reducing the stresses at equilibrium [6].

One of the drawbacks of this approach are that the feasible shape is often limited to the surface with constant stress, and the equilibrium shape obtained by actually connecting the plane sheets might be far from the specified shape. Another drawback is that the distribution of the stress after pretensioning may not be uniform as expected. The initial shape and stresses may be improved by optimizing the shape of each cutting pattern through an iterative process involving incremental and iterative deformation analysis with geometrical nonlinearity [7, 8]. In this case, however, substantial computational effort is needed if the number of membrane elements is increased.

Development of curved surfaces to plane sheets has been extensively investigated also in textile fabrication for shoes and clothes. Optimum development can be defined by minimum strain energy in the fabrication process [9–12]. There are several methods to obtain cutting patters from strip models [13, 14]. In those papers, however, no explicit condition has been utilized for flattening the surface discretized by using a finite element model.

Ohsaki *et al.* [15] and Ohsaki and Uetani [16] presented an inverse method where the conditions for the surface to be reduced to plane sheets, which are simply called *developability conditions*, are incorporated in the process of finding equilibrium shape with minimum stress deviation from the target distribution. Their method consists of two levels of optimization problems. The stresses are first optimized at the lower-level problem for the given shape of the surface under constraints on equilibrium and developability conditions. In the upper-level problem, the equilibrium shape that has been specified in the lower-level problem is optimized to further improve the stress distributions.

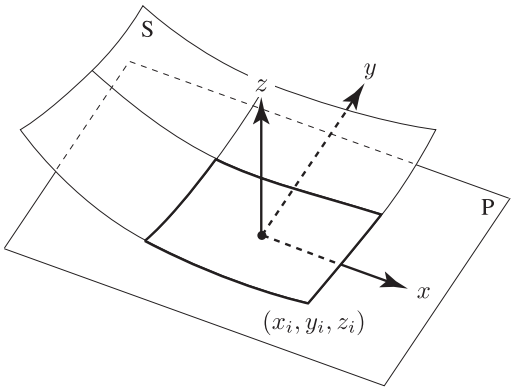

Fig. 3.1: Definition of coordinates by the tangent plane of each element.

The trade-off between shape and stress deviations can be incorporated in the objective function, if necessary. In their method, however, the surface should be discretized by triangular finite elements with uniform stresses, and the developability conditions are written in terms of stresses. Therefore, their method seems to depend strongly on the method of finite element discretization.

In this chapter, we summarize the method in Refs. [15] and [16] to present the developability conditions by local coordinates. The effectiveness of using the developability conditions is demonstrated in numerical examples.

3.2 Developability conditions by local coordinates.

Consider a surface discretized to finite elements. Let P denote a tangent plane at the center of each element. Fig. 3.1 illustrates the case of four elements. Let (x, y) denote the orthogonal coordinates on P of an element on S. The coordinate normal to P is denoted by z. The location of the ith node of the element is given as (x_i, y_i, z_i), and the derivative of z-coordinate of S in the (x, y)-directions at the ith node are written as d_{xi} and d_{yi}, respectively. Similarly, the nodal displacements in the (x, y, z)-directions are denoted by (u_i, v_i, w_i), and g_{xi} and g_{yi} denote the derivatives of displacements in z-direction at ith node with respect to x and y, respectively. The following relations should be satisfied for the curved element to be reduced to a plane:

$$w_i = -z_i \tag{3.1}$$

$$g_{xi} = -d_{xi} \tag{3.2}$$

$$g_{yi} = -d_{yi} \tag{3.3}$$

Note that compatibility along the lines or curves between the elements is not included in (3.1)-(3.3). For a given shape of S, z_i, d_{xi} and d_{yi} are to be specified, and by using (3.1)-(3.3), the unknown nodal displacements are u_i and v_i at each node. Let $\mathbf{u}^e$ denote the vector of independent components of nodal displacements after constraining the rigid body rotation and translation. If we use the standard assumption of large deformation-small strain, the strain vector at a point in the element can be defined as a linear function of $\mathbf{u}^e$ that is written as $\boldsymbol{\varepsilon}^e(\mathbf{u}^e; x, y)$. The compatibility conditions along the boundaries between the elements are given as follows by the vector $\mathbf{u}$ that consists of $\mathbf{u}^e$ of all the nodes on S.

- Compatibility of arc elongation:
  Let e_i denote the arc connecting elements a and b. The strain in elements a and b along the curve e_i between the two elements are denoted by ε^a and ε^b, respectively. Then the compatibility

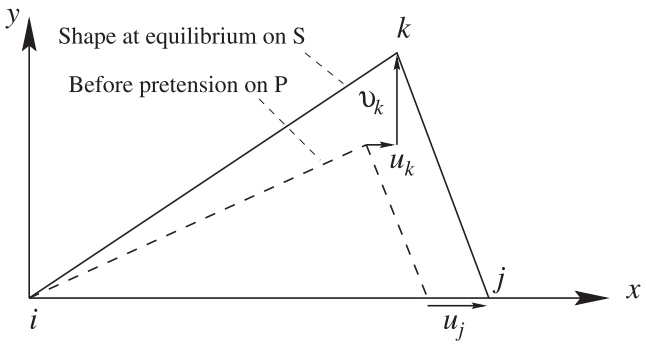

Fig. 3.2: Definition of local coordinates.

condition is written as

$$\int_{e_i} \varepsilon^a \mathrm{d}e_i = \int_{e_i} \varepsilon^b \mathrm{d}e_i \tag{3.4}$$

which may be written in the following form:

$$\mathbf{Gu} = \mathbf{0} \tag{3.5}$$

because the strain is assumed to be a linear function of the nodal displacements.

- Compatibility around a node:
  Let I denote the set of indices of the elements that connect to node c. The angle between the arcs connecting to node c of the element i on S is denoted by Θ_i^c. Since the sum of the angles around a node on P should be equal to 2π, the increment of the angle θ_i^c due to removal of the stresses should satisfy

$$\sum_{i \in I} (\Theta_i^c - \theta_i^c) = 2\pi \tag{3.6}$$

  Since the shear strain is a linear function of $\mathbf{u}$, (3.6) is simply written as

$$\mathbf{Hu} = \mathbf{h} \tag{3.7}$$

3.3 Triangular element of uniform stress.

It is shown in this section that the developability conditions of local formulation are equivalent to the conditions in terms of stresses presented in Refs. [15] and [16] if the triangular element with uniform stresses is used.

Let i, j, k denote the three nodes of an element. The local coordinates (x, y) are defined for S as shown in solid lines in Fig. 3.2 where the node i is taken as the origin. The strain vector corresponding to the local coordinates is defined as $\boldsymbol{\varepsilon}^e = \{\varepsilon_x^e, \varepsilon_y^e, \gamma_{xy}^e\}^\top$. The displacement vector $\mathbf{u}^e$ after constraining the rigid body rotation and translation is given as $\mathbf{u}^e = \{u_j, u_k, v_k\}^\top$, where u_j, u_k and v_k are as defined in Fig. 3.2. The relation between $\boldsymbol{\varepsilon}^e$ and $\mathbf{u}^e$ is given as [17]

$$\boldsymbol{\varepsilon}^e = \mathbf{C}\mathbf{u}^e \tag{3.8}$$

The constitutive relation between $\boldsymbol{\varepsilon}^e$ and the corresponding stress vector $\boldsymbol{\sigma}^e$ of the element is given as

$$\boldsymbol{\sigma}^e = \mathbf{D}\boldsymbol{\varepsilon}^e \tag{3.9}$$

From (3.8) and (3.9), $\boldsymbol{\sigma}^e$ is defined in terms of $\mathbf{u}^e$ as

$$\boldsymbol{\sigma}^e = \mathbf{D}\mathbf{C}\mathbf{u}^e \tag{3.10}$$

which is written as

$$\boldsymbol{\sigma}^e = \mathbf{F}^e\mathbf{u}^e \tag{3.11}$$

Since $\mathbf{F}^e$ is a regular matrix, $\mathbf{u}^e$ is written inversely as

$$\mathbf{u}^e = [\mathbf{F}^e]^{-1}\boldsymbol{\sigma}^e \tag{3.12}$$

Eq. (3.11) is assembled to the total surface to derive the relation

$$\boldsymbol{\sigma} = \mathbf{F}\mathbf{u} \tag{3.13}$$

The compatibility (3.4) of arc elongation is simply written as

$$\varepsilon^a = \varepsilon^b \tag{3.14}$$

and (3.5) is written in terms of $\boldsymbol{\sigma}$ as

$$\mathbf{G}\mathbf{F}^{-1}\boldsymbol{\sigma} = \mathbf{0} \tag{3.15}$$

The increments of angle is also written in linear forms of stresses under assumption of small deformation [15, 16], and the compatibility of the angle is written in terms of stresses as

$$\mathbf{H}\mathbf{F}^{-1}\boldsymbol{\sigma} = \mathbf{h} \tag{3.16}$$

3.4 Stress optimization problem.

Consider a problem of constructing a curved surface of specified shape from plane sheets so as to minimize stress deviation under equilibrium conditions and developability conditions. The equilibrium conditions are written as

$$\mathbf{S}\boldsymbol{\sigma} = \mathbf{0} \tag{3.17}$$

where $\mathbf{S}$ is the equilibrium matrix defined by the nodal coordinates on the surface.

Let $\boldsymbol{\sigma}_0$ denote the target stress vector. The optimization problem for minimizing the stress deviation is stated as follows if stresses are taken as independent variables:

$$\text{PL:} \quad \text{minimize} \quad P(\boldsymbol{\sigma}) = \frac{1}{2}(\boldsymbol{\sigma} - \boldsymbol{\sigma}_0)^\top(\boldsymbol{\sigma} - \boldsymbol{\sigma}_0) \tag{3.18}$$

$$\text{subject to} \quad (3.15) - (3.17) \tag{3.19}$$

Since PL is a quadratic programming problem with linear equality constraints, it can be solved by the Lagrangian multiplier method.

Eqs. (3.15)-(3.17) are combined to

$$\mathbf{A}\boldsymbol{\sigma} = \mathbf{a} \tag{3.20}$$

and the Lagrangian is defined as

$$\Pi = P(\boldsymbol{\sigma}) + \boldsymbol{\lambda}^\top\{\mathbf{A}\boldsymbol{\sigma} - \mathbf{a}\} \tag{3.21}$$

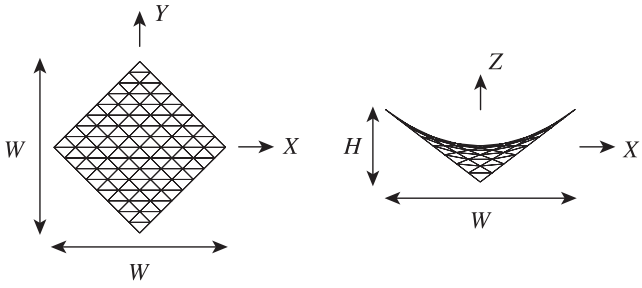

(a) Plan and elevation.

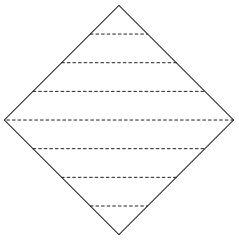

(b) Cutting pattern.

Fig. 3.3: A frame-supported HP-type membrane (Model 1).

where $\boldsymbol{\lambda}$ is the vector of Lagrange multipliers.

From the stationary conditions of Π with respect to $\boldsymbol{\sigma}$ and $\boldsymbol{\lambda}$, the following equations are derived:

$$\boldsymbol{\sigma} + \mathbf{A}^\top \boldsymbol{\lambda} = \boldsymbol{\sigma}_0 \tag{3.22}$$

$$\mathbf{A}\boldsymbol{\sigma} = \mathbf{a} \tag{3.23}$$

From (3.22),

$$\boldsymbol{\sigma} = -\mathbf{A}^\top \boldsymbol{\lambda} + \boldsymbol{\sigma}_0 \tag{3.24}$$

which is incorporated into (3.23) to lead to

$$\mathbf{A}\mathbf{A}^\top \boldsymbol{\lambda} = \mathbf{A}\boldsymbol{\sigma}_0 - \mathbf{a} \tag{3.25}$$

The multipliers $\boldsymbol{\lambda}$ are obtained from (3.25), and $\boldsymbol{\sigma}$ is to be found by incorporating them into (3.24). It is easily seen that $\boldsymbol{\sigma}$ is converted to $\mathbf{u}$ by (3.13), and the number of elements in $\boldsymbol{\sigma}$ and $\mathbf{u}$ are same if the triangular element of uniform stresses and strains are used. Therefore the same result is obtained by considering $\mathbf{u}$ as independent variables.

3.5 Examples.

In the following examples, the membrane material is orthotropic elastic and the elastic moduli in x- and y-directions are 806.05 MPa and 267.05 MPa, respectively. The shear modulus is 69.825 MPa, and the Poisson's ratio ν_{xy} is 0.90550. The thickness of membrane is 0.08 cm. The target stresses are 6.125 MPa for σ_x and σ_y, and 0 for τ_{xy}. Compatibility in the total edge length along the cutting lines is considered in the local formulation.

Consider an HP-type membrane structure (Model 1) as shown in Fig. 3.3(a), where the boundary consists of four rigid beams. The internal shape is defined as

$$Z = \frac{(X^2 - Y^2)H}{W^2} \tag{3.26}$$

Table 3.1: Optimization results (Model 1).

Stress deviation $(\text{MPa})^2$		105.2539	
Stress (MPa)	σ_x	σ_y	τ_{xy}
Average	6.1157	6.1183	0.0000
Maximum	8.0484	7.9188	1.4065
Minimum	4.0812	4.5843	−1.4065
Standard deviation	0.8603	0.8173	0.4863

Table 3.2: Result of shape analysis after regeneration of cutting patterns (Model 1).

Stress deviation $(\text{MPa})^2$		104.0868	
Stress (MPa)	σ_x	σ_y	τ_{xy}
Average	6.0271	6.0497	0.0006
Maximum	7.8916	7.8235	1.3548
Minimum	3.9391	4.4416	−1.3471
Standard deviation	0.8495	0.8176	0.4701

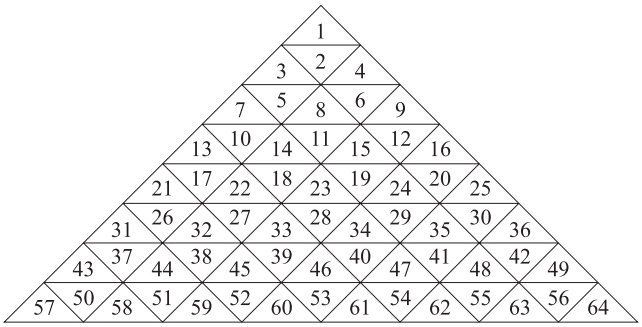

Fig. 3.4: Element numbers for Model 1.

where $W = 32.0$ m and $H = 6.4$ m in the following example. The membrane is divided into eight sheets, and optimization is carried out for a half of the surface by considering symmetry conditions. The cutting pattern is as shown in dotted lines in Fig. 3.3(b). The warp direction of each element coincides with the edge that is closest to the X-direction, and the fill (weft) direction is normal to the warp direction; i.e., the effect of shear deformation is neglected in the process of defining the directions of fabrics at equilibrium. The plane P for global formulation is the XY-plane for all the cutting sheets.

The optimization results as shown in Table 3.1. The element numbers are assigned as shown in Fig. 3.4 for those in $Y \geq 0$. Figs. 3.5(a)-(c) show the equilibrium shape, the optimal shapes of plane sheets and the optimal stresses, respectively. It can be seen fron this result that a shape with small stress deviation can be found by the propose method.

Since the developability conditions used in the local formulation is a linear approximation that is valid for small strains, there exist slight errors in the unstressed shape of the elements. Therefore, the cutting patterns should be regenerated as follows before carrying out shape analysis for verification purpose:

1. Find the optimal stresses based on the local formulation.

2. Remove the stresses of all the elements independently to obtain pieces of unstressed triangles.

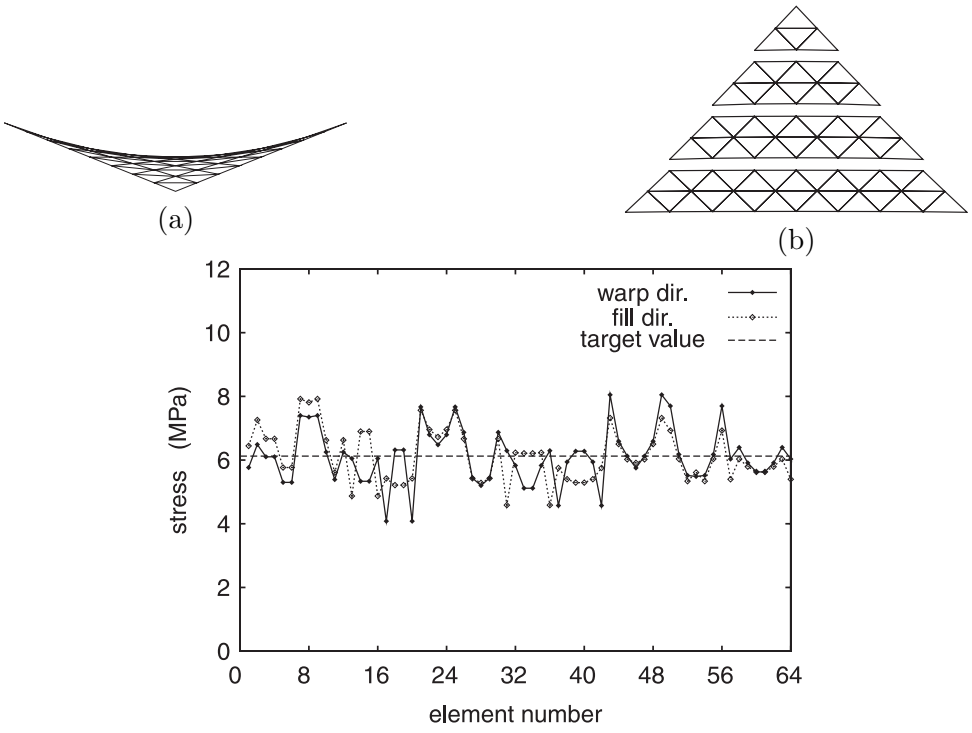

(c)

Fig. 3.5: Optimization results by local formulation (Model 1): (a) equilibrium shape, (b) cutting pattern, (c) stresses.

3. Place a triangle on a plane.

4. Find a triangle of which locations of two nodes are already defined.

5. Adjust the length of the edge between the two nodes with the lengths of remaining two edges unchanged, and place the triangle on the plane.

6. Insert an edge between two nodes that are already placed on the plane and are not connected.

7. Go to 3 if all the triangles have not been placed.

The results of shape analysis for the optimum stresses are as shown in Table 3.2. The stress distributions are also plotted in Fig. 3.6. It is seen from Table 3.2 that the stresses are fairly equal to those in Table 3.1, which means that the errors due to linear approximation is negligibly small, and the stress distributions that are close to the optimal values can be attained.

Consider next a frame-supported membrane (Model 2) as shown in Fig. 3.7 that has larger curvature and more complex surface than Model 1. The geometrical parameters are $w = 4.0$ m, $h_1 = 1.5$ m and $h_2 = 1.0$ m. The boundaries are assumed to be rigid, and the internal shape has been obtained by shape analysis for the given target stresses. The membrane consists of ten triangular parts, each of which is divided into two cutting sheets as shown in Fig. 3.7(c). The warp direction of each element coincides with the edge that is closest to the X^*-direction defined in Fig. 3.8 for each triangular part.

The optimization results are as shown in Table 3.3. The element numbers are assigned as shown in Fig. 3.9. The optimal shapes of plane sheets and the optimal stresses are as shown in Figs. 3.10. It is seen from these results that the shape with small stress deviations can be found by the proposed.

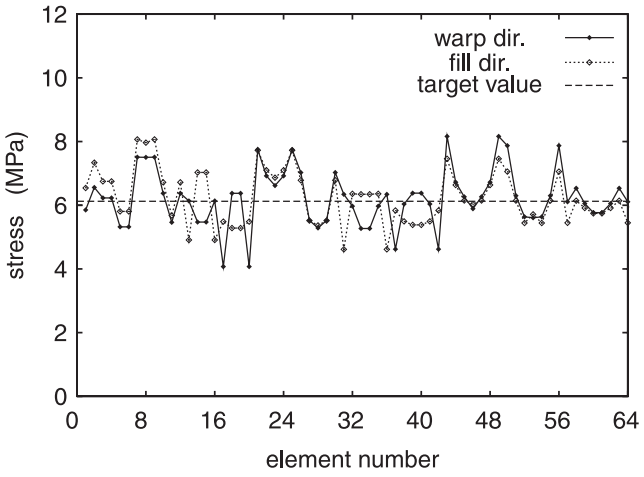

Fig. 3.6: Result of shape analysis for the optimal solution by local formulation (Model 1).

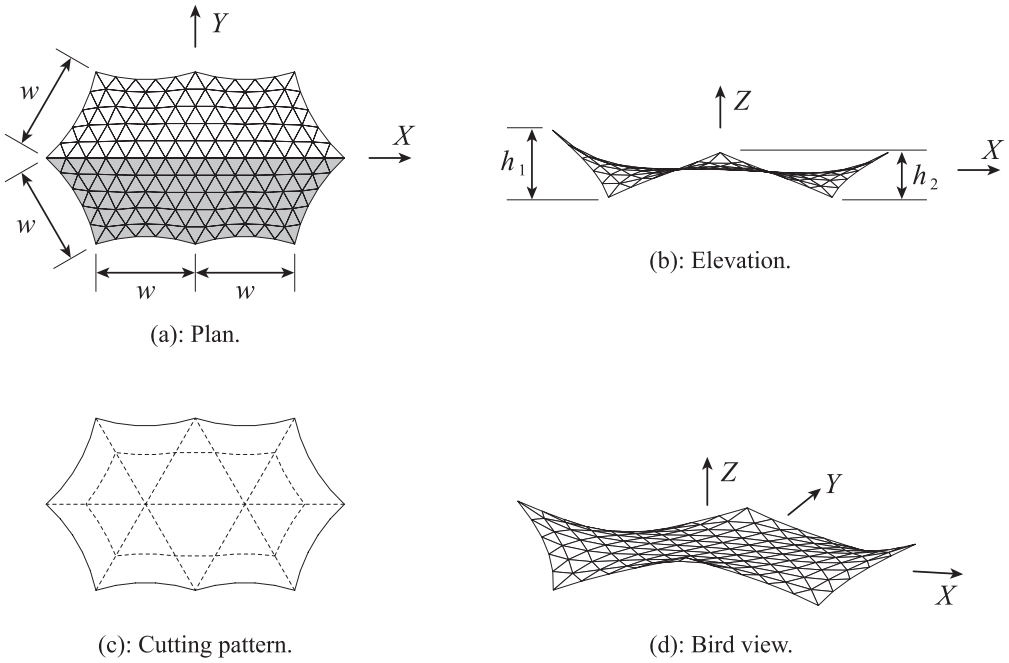

Fig. 3.7: A frame-supported membrane (Model 2).

The results of shape analysis after regeneration of the cutting patterns are listed in Table 3.4. The stress distributions are as shown Fig. 3.11. It is seen from Table 3.4 that the stresses are fairly equal to those in Table 3.3.

3.6 Conclusions.

General formulations have been presented for developability conditions of surfaces to plane sheets based on the displacements in the local coordinates. It has been shown that the conditions based on the local formulation are extension of those by Ohsaki *et al.* [15] and Ohsaki and Uetani [16], where the stresses are defined in terms of local displacements and the unstressed shapes of the triangular elements are found by releasing the stresses at equilibrium.

The developability conditions have been applied to an optimization problem for minimizing stress

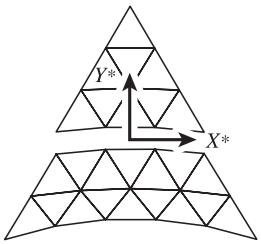

Fig. 3.8: Local coordinates (X^*, Y^*) for defining warp and fill directions (Model 2).

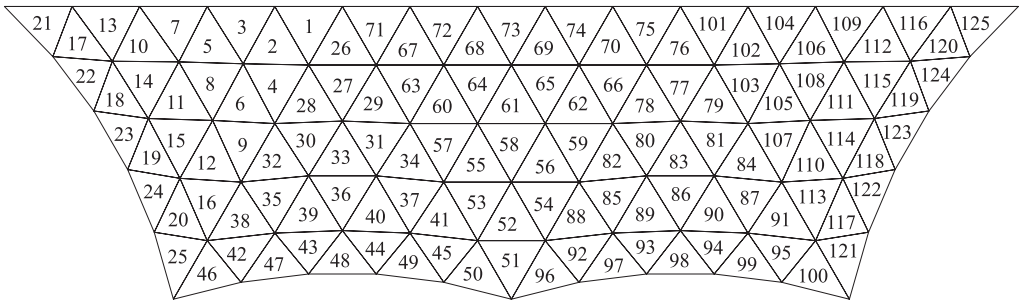

Fig. 3.9: Element numbers for Model 2.

Table 3.3: Optimization results (Model 2).

Stress deviation $(\text{MPa})^2$		55.1235	
Stress (MPa)	σ_x	σ_y	τ_{xy}
Average	6.1311	6.1251	0.0035
Maximum	7.9364	6.7655	0.4371
Minimum	4.8519	5.2822	−0.4186
Standard deviation	0.5809	0.2876	0.1442

Table 3.4: Result of shape analysis after regeneration of cutting patterns (Model 2).

Stress deviation $(\text{MPa})^2$		60.3382	
Stress (MPa)	σ_x	σ_y	τ_{xy}
Average	6.2733	6.2388	0.0031
Maximum	8.1066	6.9113	0.4418
Minimum	4.9530	5.3753	−0.4224
Standard deviation	0.5813	0.2987	0.1435

deviation of a finite element model from the target values. Since any arbitrary shape cannot be realized by simply stretching the plane sheets, there is an upper bound in number of elements for discretizing the surface.

The performances of the proposed formulations have been investigated in the numerical examples. It has been shown that the stresses can be estimated fairly accurately by the proposed formulation; i.e. the stress obtained from the regenerated cutting patterns are very close to the optimal stresses.

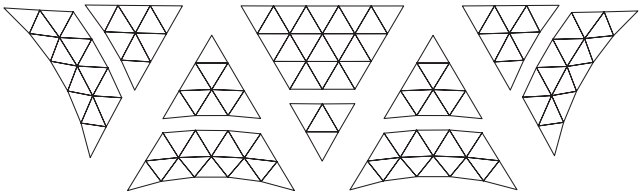

(a)

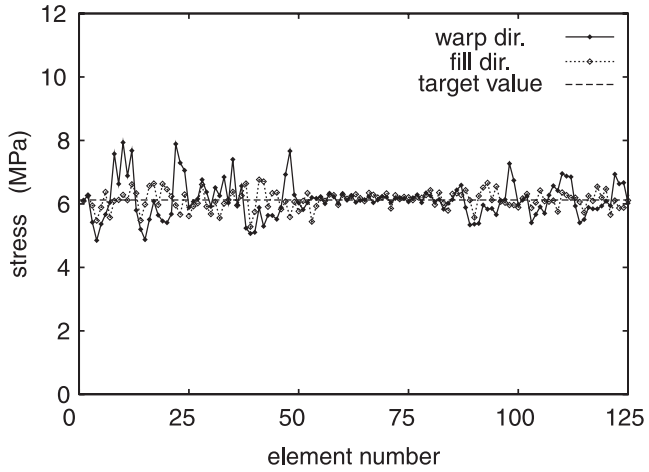

(b)

Fig. 3.10: Optimization results (Model 2): (a) cutting pattern, (b) stresses.

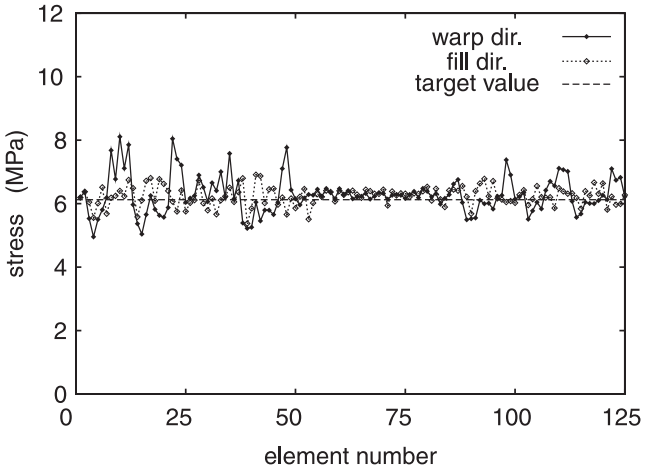

Fig. 3.11: Result of shape analysis for the optimal solution (Model 2).

References

[1] R.B. Harber and J.F. Abel: Initial equilibrium solution methods for cable reinforced members, Part I – Formulations, Comp. Meth. Appl. Mech. Engng, Vol. 30, pp263-284, 1982.

[2] M.R. Barnes, Form-finding and analysis of prestresses nets and membranes, Comp. & Struct., Vol. 30, pp685-695, 1988.

[3] M. Hinata, M. Shimasaki and T. Kiyono, Numerical solution of Plateu's problem by a finite element method, Math. Comp., Vol. 28, pp45-60, 1974.

[4] Z. Sobotka, Optimization of shells for the membrane state, ACTA Technica ČSAV, No. 6, pp745-773, 1989.

[5] H.-J. Schek, The force density method for form finding and computation of general networks, Comp. Meth. Appl. Mech. Engng., Vol. 3, pp115-134, 1974.

[6] J.L. Meek and K.Y. Tan: Post-formfinding determination of geodesic lines in cutting pattern design for membrane structures, Space Struct., Vol. 2, pp231-239, 1986.

[7] H. Tsubota and A. Yoshida, Theoretical analysis of determining optimum cutting patterns for membrane structures, Proc. IASS Symposium, Madrid, Vol. 3, pp. 11-15, 1989.

[8] J-Y. Kim and J-B. Lee, A new technique for optimum cutting pattern generation of membrane structures, Engng. Struct., Vol. 24, pp. 745-756, 2002.

[9] G. Yu, N. M. Patrikalakis and T. Maekawa, Optimal development of doubly curved surfaces, Comp. Aided Geog. Des., Vol. 17, pp. 545-577, 2000.

[10] J. McCartney, B. K. Hinds and B. L. Seow, The flattening of triangulated surfaces incorporating darts and gussets, Comp. Aided Des., Vol. 31, pp. 249-260, 1999.

[11] T. Shimada and Y. Tada, Approximate transformation of an arbitrary curved surface into a plane using dynamic programming, Comp. Aided Des., Vol. 23(2), pp. 153-159, 1990.

[12] C. C. L. Wang, S. S-F. Smith and M. M. F. Yuen, Surface flattening based on energy model, Comp. Aided Des., Vol. 34, pp. 823-833, 2002.

[13] B. K. Hinds, J. McCartney and G. Woods, Pattern development for 3D surfaces, Comp. Aided Des., Vol. 23(8), pp. 583-592, 1991.

[14] P. Azariadis and N. Aspragathos, Design of plane developments of doubly curved surfaces, Comp. Aided Des., Vol. 29(10), pp. 675-685, 1996.

[15] M. Ohsaki, K. Uetani and S. Takatani, Shape-stress trade-off design method of membrane structures by using inverse problem approach, J. Struct. Constr. Eng., AIJ, No. 488, pp107-115, 1996. (in Japanese)

[16] M. Ohsaki and K. Uetani, Shape-stress trade-off design of membrane structures for specified sequence of boundary shapes, Comp. Meth. Appl. Mech. Engng., Vol. 182, pp. 73-88, 2000.

[17] O.C. Zienkiewicz, The Finite Element Method, McGraw Hill, 1989.

Chapter 4

Structural Optimization for Specified Nonlinear Buckling Load Factor

4.1 Introduction.

In the design process of dome structures and high-rise buildings, it is important to assign appropriate cross-sectional properties of members so that the structures have enough safety considering instability against possible large design loads. In the field of structural engineering, such an instability phenomenon is called buckling. For column-type structures such as transmission towers and high-rise buildings, linear eigenvalue formulation is usually applied in the design process because the effect of deformation before buckling, which is called prebuckling deformation, is negligible. For shallow dome structures, however, the effect of prebuckling deformation is usually to be incorporated in evaluating the buckling loads. In this chapter, we consider an optimization problem for determining the stiffness distribution of an elastic finite dimensional structure under nonlinear buckling constraints. The applied loads are quasi-static and proportional, and are defined by the parameter called load factor.

Optimization of structures for specified linear buckling load factor has been extensively investigated including the case where the optimum design has multiple or repeated eigenvalues [1–5]. Recently, there have also been many studies for optimum design for specified nonlinear buckling load factor considering prebuckling deformation [6–10].

Nonlinear buckling of a structure is defined as a critical point of the equilibrium path which is classified into a limit point and a bifurcation point as shown briefly in the following section. It is easy to find optimum designs for specified limit point load factor by using a gradient based mathematical programming approach, because the sensitivity coefficients of the limit point load factor with respect to the design variables such as cross-sectional areas and nodal coordinates are bounded [10]. For a symmetric structure subjected to symmetric proportional loads, the sensitivity coefficients of bifurcation load factor are not bounded for an asymmetric modification of design variables which is classified as major imperfection [11]. On the contrary, a symmetric design modification is classified as minor imperfection [12] where the sensitivity coefficients are bounded even for a bifurcation point. Ohsaki and Uetani [13] presented a method of finding sensitivity coefficients of the bifurcation load factor of a symmetric structure, and applied it to optimum design of trusses [17].

It is well known that an optimum design under buckling constraints often has multiple critical load factors. In this case, it is very difficult to obtain the optimal solution even for linear buckling load constraints [5]. In the field of nonlinear stability analysis, critical points with multiple null eigenvalues of tangent stiffness matrix are called coincident critical points [16]. Although it have been suggested by Thompson and Hunt [14] that the maximum load factor should be carefully determined for the case of coincident critical points, some researchers believe that obtaining such a structure is meaningless. Recently, the author has presented sensitivity analysis and optimization

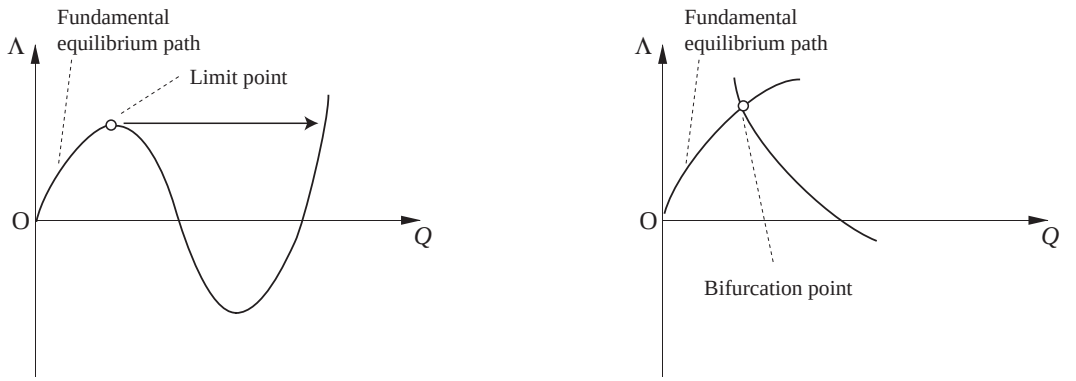

(a) Limit point. (b) Bifurcation point.

Fig. 4.1: Equilibrium path in $(\mathbf{Q}, \Lambda)$-space and classification of critical points.

methods for problems with coincident critical load factors, and showed some examples of a small truss [15]. To the author's knowledge, no method of has been presented for sensitivity analysis and optimization corresponding to coincident nonlinear critical points of a moderately large structure with practically acceptable number of degrees of freedom.

In this chapter, the author's method of design sensitivity analysis and optimization of geometrically nonlinear structures are applied to a truss with moderately large number of degrees of freedom. The results are compared with those by linear eigenvalue formulation, and the imperfection sensitivity properties of the optimal designs are discussed in detail.

4.2 Nonlinear stability analysis.

Consider a finite dimensional elastic conservative system where the equilibrium state is determined by stationary condition of the total potential energy. The structure is subjected to a set of quasi-static proportional loads $\mathbf{P} \in R^f$ defined by the constant vector $\mathbf{P}^0 \in R^f$ and the load factor Λ as $\mathbf{P} = \Lambda \mathbf{P}^0$, where f is the number of degrees of freedom. The vector of state variables such as nodal displacements is denoted by $\mathbf{Q} \in R^f$. The total potential energy $\Pi(\mathbf{Q}, \Lambda)$ is a function of $\mathbf{Q}$ and Λ.

Let S_i denote partial differentiation of Π with respect to Q_i. Stationary condition of Π with respect to Q_i leads to the following equilibrium equations:

$$S_i = 0, \quad (i = 1, 2, \cdots, f) \tag{4.1}$$

The trajectory of equilibrium state in $(\mathbf{Q}, \Lambda)$-space is called equilibrium path. The path that originates the undeformed initial state is called fundamental equilibrium path as illustrated in Fig. 4.1. Let t denote a parameter that defines a point along the equilibrium path. t may represent Λ, Q_i, or the arc-length of the path, and is written in general form as

$$t = g(\mathbf{Q}, \Lambda) \tag{4.2}$$

The Hessian of Π with respect to Q_i is denoted by $\mathbf{S} = [S_{ij}] \in R^{f \times f}$ which is called stability matrix or tangent stiffness matrix. The rth eigenvalue $\lambda_r(t)$ and eigenvector $\Phi_r(t) = \{\phi_{ri}(t)\} \in R^f$ of $\mathbf{S}(t)$ along the fundamental equilibrium path are defined by

$$\sum_{j=1}^{f} S_{ij}\phi_{rj} = \lambda_r \phi_{ri}, \quad (i = 1, 2, \cdots, f) \tag{4.3}$$

where Φ_r is normalized by

$$\sum_{j=1}^{f}(\phi_{rj})^2 = 1 \tag{4.4}$$

Note that the eigenvalues λ_r are numbered in increasing order; i.e. λ_1 is the lowest eigenvalue.

An equilibrium state that satisfies (4.1) is stable if $\lambda_1 > 0$, and is unstable if $\lambda_1 < 0$. The value of Λ corresponding to $\lambda_1 = 0$ is called critical load factor or buckling load factor, and such an equilibrium state indicated by $t = t^{\mathrm{c}}$ is called critical point. In the following, the values corresponding to $t = t^{\mathrm{c}}$ is denoted by a superscript $(\ )^{\mathrm{c}}$.

The critical points are classified into limit points and bifurcation points as illustrated in Fig. 4.1. At a limit point, a so called snap-through takes place to a stable equilibrium state as shown in Fig. 4.1(a). At a bifurcation point, there exists a branch that bifurcates from the critical point. A parameter β is defined by

$$\beta = \sum_{j=1}^{f}\phi_{1j}^{\mathrm{c}}P_j^0 \tag{4.5}$$

For the case where S_{ij} does not depend explicitly on Λ, the critical points are classified by using β as [14]

$$\text{Limit point:} \quad \beta \neq 0 \tag{4.6}$$

$$\text{Bifurcation point:} \quad \beta = 0 \tag{4.7}$$

4.3 Optimum design problem.

Consider a truss defined by the vector of cross-sectional areas $\mathbf{A} = \{A_i\}$. The upper and lower bounds for A_i are denoted, respectively, by A_i^U and A_i^L. The specified lower bound of the critical load factor Λ^{c} is denoted by $\bar{\Lambda}^{\mathrm{c}}$. For the case of coincident buckling, the buckling constraint may be written as

$$\Lambda_j^{\mathrm{c}}(\mathbf{A}) \geq \bar{\Lambda}^{\mathrm{c}}, \quad (j = 1, 2, \cdots, s) \tag{4.8}$$

where Λ_j^{c} is the jth buckling load factor along the fundamental equilibrium path, and s is the sufficiently large number for possible multiplicity. In this case, the buckling load factors of sufficient number should be obtained at each step of optimization. For the initial solution, however, $\Lambda_2^{\mathrm{c}}, \Lambda_3^{\mathrm{c}}, \ldots, \Lambda_s^{\mathrm{c}}$ may be far above Λ_1^{c}, and substantial computational effort is needed for finding all the necessary buckling load factors and their design sensitivity coefficients by tracing the fundamental equilibrium path.

Therefore, the optimization problem for minimizing the objective function $C(\mathbf{A})$ is formulated as [15]

$$\text{Minimize} \quad C(\mathbf{A}) \tag{4.9}$$

$$\text{subject to} \quad \Lambda_j^{\mathrm{c}}(\mathbf{A}) \geq \bar{\Lambda}^{\mathrm{c}}, \quad (j = 1, 2, \cdots, q) \tag{4.10}$$

$$\lambda_r^{\mathrm{c}}(\mathbf{A}) \geq 0, \quad (r = q+1, q+2, \cdots, s) \tag{4.11}$$

$$A_i^L \leq A_i \leq A_i^U \tag{4.12}$$

where q is the multiplicity of the critical load factor of the current design during optimization. In this case, the path-following analysis can be terminated at the first critical point.

In the following examples, the optimization problem is solved by using a standard gradient-based approach, where design sensitivity analysis is carried out by the method proposed in [15].

Table 4.1: Nodal coordinates (cm) of the spherical truss.

Node number	x	y	z
1	0.0	0.0	461.880
2	239.087	0.0	430.404
3	119.543	207.055	430.404
4	461.880	0.0	338.120
5	400.0	230.940	338.120
6	230.940	400.0	338.120
7	653.197	0.0	191.317
8	613.805	223.407	191.317
9	500.378	419.867	191.317
10	326.599	565.685	191.317
11	800.0	0.0	0.0
12	772.741	207.055	0.0
13	692.820	400.0	0.0
14	565.685	565.685	0.0
15	400.0	692.820	0.0

Table 4.2: Total volumes and critical load factors of the optimum designs.

	Concentrated load (Case 1)	Distributed load (Case 2)
Volume ($\times 10^6 \mathrm{cm}^3$)	1.2677	3.0704
Λ_1^c	99.961	99.998
Λ_2^c	99.952	100.409
Λ_3^c	99.728	100.409
Λ_4^c	–	101.148
Λ_5^c	–	101.148
Λ_6^c	–	102.340
Linear buckling load	228.153	135.230

4.4 Examples.

Optimum designs are found for a spherical truss as shown in Fig. 4.2. The radius of the circle where the supports are located is 800.0 cm, and the height is 461.880 cm. The coordinates of the nodes in one of the six equal parts as numbered in Fig. 4.3 are listed in Table 4.1. The objective function is the total structural volume. A_i^L is equal to 1.0 cm^2 for all the members, and A_i^U is not given. The elastic modulus of the members is 205.8 GPa. Based on the symmetry property, the members are divided into 14 groups of which members have the same cross-sectional area.

Lagrangian formulation with Green's strain is used for defining the strain-displacement relation [22]. The total potential energy has been symbolically differentiated by using Maple V Release 5 [23]. The fundamental equilibrium path is traced by the displacement increment method. The specified buckling load factor is 100.0. Optimum designs are found by the method of modified feasible direction [24].

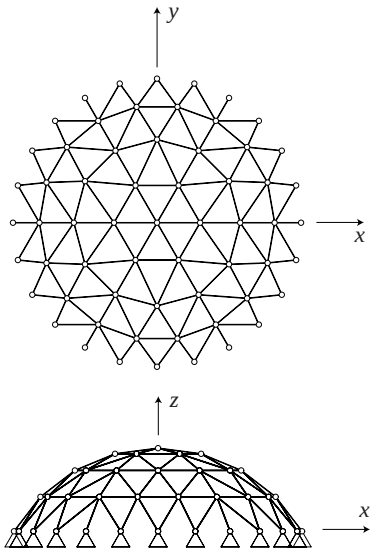

Fig. 4.2: A spherical truss.

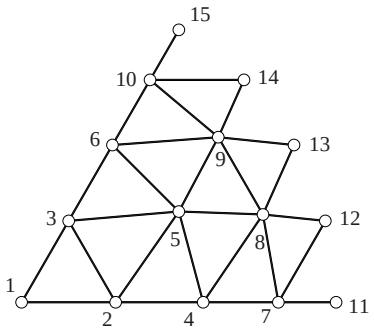

Fig. 4.3: Node numbers of the spherical truss.

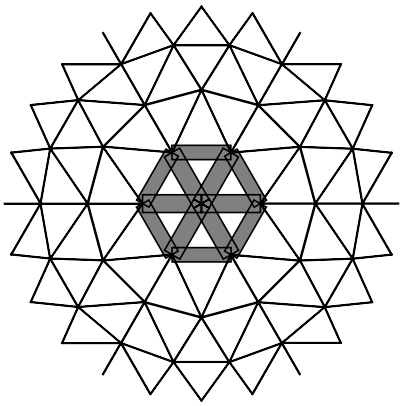

Fig. 4.4: Optimum design for concentrated load (Case 1).

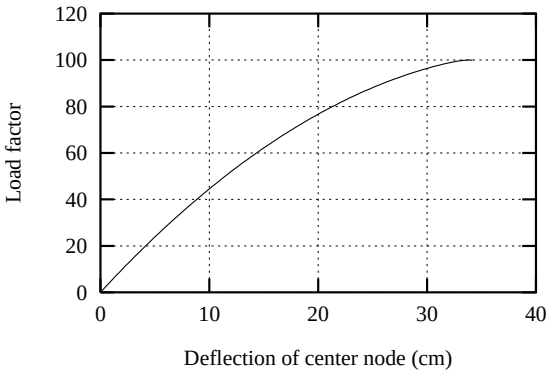

Fig. 4.5: Relation between deflection of center node and load factor (Case 1).

4.4.1 Case 1: concentrated load

Consider Case 1, where a nodal load ΛP^0 with $P^0 = 9.8$ kN is applied in the negative z-direction of the center node. The optimal cross-sectional areas are as shown in Fig. 4.4, where the width of each member is proportional to its cross-sectional area. It is observed from Fig. 4.4 that the members near the center have large cross-sectional areas. The total volume and the first three buckling load factors along the fundamental equilibrium path are as listed in the first column of Table 4.2. Note that three buckling load factors are closely located at the optimum design. The values of β of the modes corresponding to three critical points have been computed from (4.5) to find that a limit point and two bifurcation points almost coincide. Note for this case that S_{ij} does not explicitly depend on Λ. Let $t_j^{\rm c}$ denote the value of t at $\Lambda_j^{\rm c}$. In this example, a limit point is reached at $t = t_1^{\rm c}$, and Λ decreases as t is increased from $t_1^{\rm c}$. Then two symmetric bifurcation points are found slightly beyond the limit point. Therefore, $\Lambda_2^{\rm c}$ and $\Lambda_3^{\rm c}$ are a little less than $\Lambda_1^{\rm c}$ as observed in Table 4.2.

The linear buckling load factor of the optimum design is 228.153 which is more than twice of the specified nonlinear buckling load factor. The deflection δ of the center node at buckling is 33.7296 cm. Therefore, prebuckling deformation is very large and should be properly incorporated in evaluating

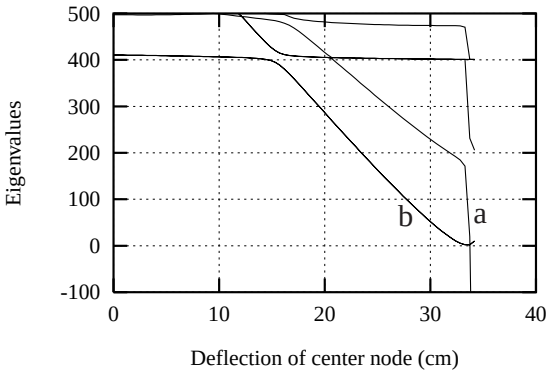

Fig. 4.6: Relation between deflection of center node and eigenvalues (Case 1).

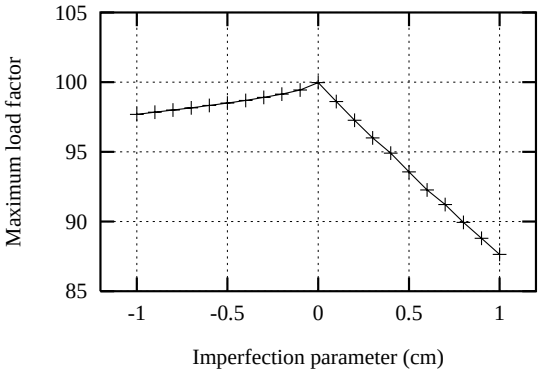

Fig. 4.7: Imperfection sensitivity for the limit-point-type mode of Case 1

the buckling loads of a single-layer spherical truss as shown in Fig. 4.2 subjected to a concentrated load. Λ and λ_r are plotted with respect to δ, respectively, in Figs. 4.5 and 4.6. Note that the curve a in Fig. 4.6 corresponds to a limit point. The curve b is duplicate and corresponds to bifurcation points. This type of coincident buckling is called hill-top branching [14].

Fig. 4.7 is the plot of maximum loads of imperfect systems. The nodes are dislocated in the direction of the symmetric buckling mode corresponding to the limit-point-type instability, where the mode is normalized so that the maximum absolute value of the components is equal to 1. The horizontal axis is the imperfection parameter c which is the scaling factor to be multiplied to the normalized mode. For $c > 0$, the imperfection of the center node is in the negative z-direction, and the critical point of the imperfect system is a limit point. In this case, the imperfection sensitivity coefficient is bounded. For $c < 0$, the critical point is a bifurcation point and this type of imperfection corresponds to a minor imperfection [12]. Therefore, the imperfection coefficients are also bounded even for the maximum load factors defined by the bifurcation points.

Fig. 4.8 shows the imperfection sensitivity in the direction of the antisymmetric buckling mode corresponding to the bifurcation-type instability. In this case, the imperfection corresponds to a major imperfection, and the imperfection coefficients are not bounded at $c = 0$. It should be noted, however, the magnitude of reduction of maximum load factor for this case is in the same order as symmetric imperfection in a finite range, e.g. $c = 1$ cm, of the imperfection parameter. Therefore, imperfection sensitivity at the perfect system corresponding to $c = 0$ is not important in practical situation, and minor imperfection should be properly considered in evaluating the maximum loads of imperfect systems.

Fig. 4.9 shows the imperfection sensitivity in the direction of the limit-point-type mode of the initial design with $A_i = 20.0$ cm^2 for all the members. Since the critical point is a simple limit point, the maximum load factor is linear with respect to the imperfection parameter. The reduction of the maximum load, e.g., for $c = 1$ cm is in the same order as that for the optimum design. Therefore the imperfection sensitivity does not increase as a result of optimization. Note that interaction between the modes corresponding to two symmetric bifurcation points as demonstrated through the Augusti model [14] has not been observed.

An optimum design has been also found under linear buckling constraints by using the semi-definite programming approach proposed in Ref. [21]. The total structural volume is 2.75730×10^5 cm^3, and the nonlinear buckling load factor of the optimum design is 21.6916. Let $\mathbf{A}^{\mathrm{NL}}$ and $\mathbf{A}^{\mathrm{LIN}}$ denote the optimum cross-sectional areas, respectively, under nonlinear and linear buckling constraints. Note that $\mathbf{A}^{\mathrm{LIN}}$ is almost proportional to $\mathbf{A}^{\mathrm{NL}}$ which has been shown in Fig. 4.4. If we scale $\mathbf{A}^{\mathrm{LIN}}$ to satisfy $\Lambda_1^{\mathrm{c}} = 100$, then the total volume is 1.27224×10^6 cm^3 which is only slightly more than that of $\mathbf{A}^{\mathrm{NL}}$ as shown in Table 4.2. Therefore, for this case, it is practically acceptable to

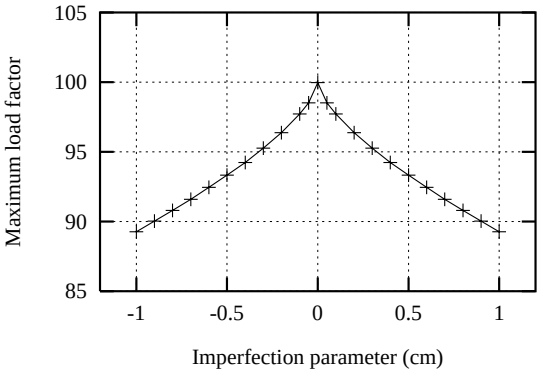

Fig. 4.8: Imperfection sensitivity for the bifurcation-type mode of Case 1

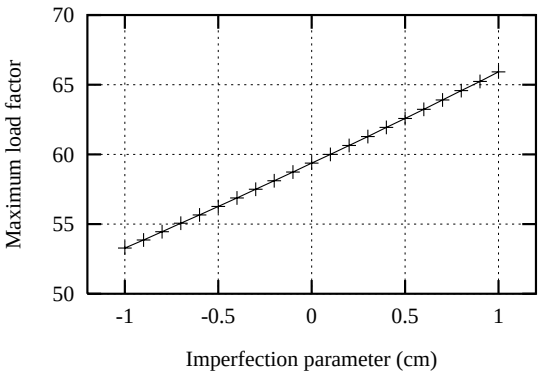

Fig. 4.9: Imperfection sensitivity of initial solution.

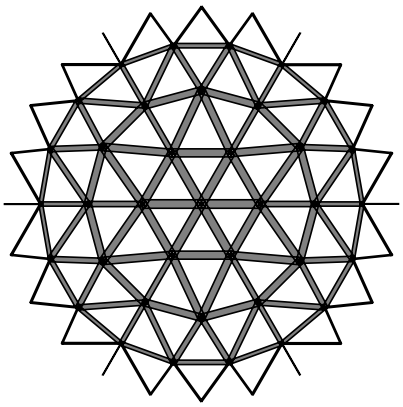

Fig. 4.10: Optimum design for distributed load (Case 2).

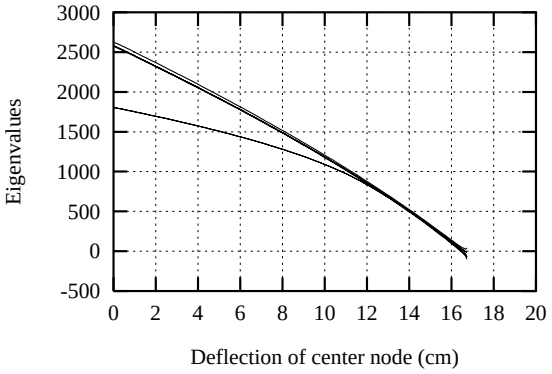

Fig. 4.11: Relation between deflection of center node and eigenvalues (Case 2).

obtain an optimum design under linear buckling constraint and just scale it up to have approximate optimum design under nonlinear buckling constraints.

4.4.2 Case 2: distributed loads

The optimal cross-sectional areas for Case 2 where the nodal load ΛP^0 with $P^0 = 9.8$ kN is distributed in the negative z-direction of each node is as shown in Fig. 4.10. It is observed from Fig. 4.10 that the cross-sectional areas are almost uniformly distributed except those for the members connected to the supports. The total volume and the first six critical load factors are as listed in the second column of Table 4.2. The linear buckling load factor of the optimum design is 109.866 which exceeds the specified nonlinear buckling load factor only about 10 %. Therefore, the effect of prebuckling deformation is not very large for the case of distributed loads. The value of δ is 16.4354 cm which is about half of that of Case 1. In Case 2, however, the deflection of each node at buckling is almost proportional to the height at the undeformed state, whereas only the nodes around the center moves in Case 1. Therefore the effect of prebuckling deformation in Case 1 is larger than that in Case 2.

The total structural volume and the nonlinear buckling load factor of $\mathbf{A}^{\mathrm{LIN}}$ is $1.90953 \times 10^5 \mathrm{cm}^3$ and 622.270, respectively. Note that $\mathbf{A}^{\mathrm{LIN}}$ is similar to $\mathbf{A}^{\mathrm{NL}}$ which has been shown in Fig. 4.10. If we scale $\mathbf{A}^{\mathrm{LIN}}$ to satisfy $\Lambda_1^{\mathrm{c}} = 100$, then the total volume is $3.06865 \times 10^6 \mathrm{cm}^3$ which is slightly smaller than that for the nonlinear buckling constraints. This result suggests that the optimization process

for nonlinear buckling constraints did not converge to a strictly optimal solution, and it is desirable to obtain the design under linear buckling constraints and scale it up to have the optimum design in a good accuracy because the prebuckling deformation for this case is not dominant in practical sense.

The relation between δ and λ_r is as shown in Fig. 4.11. In this case, six buckling load coefficients have almost same values, and the sixth critical point is a limit point. It should be noted, however, that the closely spaced value of Λ_j^c does not mean coincidence of the critical point around a limit point, because Λ takes a local maxima along the equilibrium path at the limit point, and Λ at different points along the path may have closely spaced values.

4.5 Conclusions.

The conclusions drawn from the present paper are as follows:

1. The author's method of design sensitivity analysis of coincident nonlinear critical loads and the formulation of optimum design under nonlinear buckling constraints are applicable to a finite dimensional system with moderately large degrees of freedom.

2. Optimum designs with closely spaced critical points can be found without any difficulty for a spherical truss.

3. For optimal spherical trusses exhibiting hill-top branching, the buckling modes do not interact strongly with each other because the closely located critical points are a limit point and symmetric bifurcation points. It has also been confirmed that interaction between symmetric bifurcation points as demonstrated through the Augusti model [14] does not exist in the examples of the spherical truss. Based on numerical experiments for dome-type trusses, the optimum designs tend to exhibit hill-top branching. Therefore, if a special method can be developed for finding optimum designs with hill-top branching, it will reduce the costs for optimizing the dome-type structures.

4. The magnitude of reduction of maximum load factor due to a symmetric imperfection that is classified as minor imperfection may be in the same order as that due to an antisymmetric imperfection that is classified as major imperfection. Therefore, the fact that the imperfection sensitivity of the bifurcation load factor is unbounded is not important in practical situation. Minor imperfection should be properly considered in evaluating the maximum loads of imperfect systems.

5. The optimum designs under linear and nonlinear buckling constraints are almost same for the case of distributed loads where the effect of prebuckling deformation is small. Although the effect of prebuckling deformation is very large for a spherical truss that carries a concentrated nodal load, an approximate optimum design may successfully be obtained by scaling the optimum design under constraints on linear buckling loads. Therefore, in practical point of view, computational cost can be reduced by only using the linear formulation. It is desired that numerical experiments should be carried out for many other structures to confirm the applicability of the approximate method.

References

[1] N. S. Khot, V.B. Venkayya and L. Berke, 'Optimum structural design with stability constraints,' *Int. J. Numer. Meth. Engng.* **10**, 1097-1114 (1976).

[2] R. Levy and H. Perng, 'Optimization for nonlinear stability,' *Comp. & Struct.*, **30(3)**, 529-535 (1988).

[3] N. Olhoff and S.H. Rasmussen, 'On single and bimodal optimum buckling loads of clamped columns,' *Int. J. Solids Struct.*, **13**, 605-614 (1977).

[4] E. J. Haug and K.K. Choi, 'Systematic occurrence of repeated eigenvalues in structural optimization,' *J. Optimization Theory and Appl.*, **38**, 251-274 (1982).

[5] A. P. Seyranian, E. Lund and N. Olhoff, 'Multiple eigenvalues in structural optimization problem,' *Structural Optimization*, **8**, 207-227 (1994).

[6] N. S. Khot and M. P. Kamat, 'Minimum weight design of truss structures with geometric nonlinear behavior,' *AIAA J.*, **23**, 139-144 (1985).

[7] R. H. Plaut, P. Ruangsilasingha and M. P. Kamat, 'Optimization of an asymmetric two-bar truss against instability,' *J. Struct. Mech.*, **12(4)**, 465-470 (1984).

[8] M. P. Kamat, N. S. Khot and V. B. Venkayya, 'Optimization of shallow trusses against limit point instability,' *AIAA J.*, **22(3)**. 403-408 (1984).

[9] C. C. Wu and J. S. Arora, 'Design sensitivity analysis of non-linear buckling load,' *Comp. Mech.*, **3**, 129-140 (1988).

[10] M. Ohsaki and T. Nakamura, 'Optimum design with imperfection sensitivity coefficients for limit point loads,' *Structural Optimization*, **8**, 131-137 (1994).

[11] J. M. T. Thompson, 'A general theory for the equilibrium and stability of discrete conservative systems,' *ZAMP*, **20**, 797-846 (1969).

[12] J. Roorda, 'On the buckling of symmetric structural systems with first and second order imperfections,' *Int. J. Solids Struct.*, **4**, 1137-1148 (1968).

[13] M. Ohsaki and K. Uetani, 'Sensitivity analysis of bifurcation load of finite dimensional symmetric systems,' *Int. J. Num. Meth. Engng.*, **39**, 1707-1720, (1996).

[14] J. M. T. Thompson and G.W. Hunt, *Elastic Instability Phenomena*, John Wiley and Sons, 1984.

[15] M. Ohsaki, 'Optimization of geometrically nonlinear symmetric systems with coincident critical points,' *Int. J. Numer. Meth. Engng.*, **48**, 1345-1357, (2000).

[16] D. Ho, 'Buckling load of nonlinear systems with multiple eigenvalues,' *Int. J. Solids Structures*, **10**, 1315-1330, (1974).

[17] M. Ohsaki, K. Uetani and M. Takeuchi, 'Optimization of imperfection-sensitive symmetric systems for specified maximum load factor,' *Comp. Meth. Appl. Mech. Engng.*, **166**, 349-362, (1998).

[18] C. C. Wu and J. S. Arora, 'Design sensitivity analysis and optimization of nonlinear structural response using incremental procedure,' *AIAA J.*, **25(8)**, 1118-1125, (1986).

[19] J. S. Park and K. K. Choi, 'Design sensitivity analysis of critical load factor for nonlinear structural systems,' *Comp. & Struct.*, **36(5)**, 823-838, (1990).

[20] H. Noguchi and T. Hisada, 'Development of a sensitivity analysis method for nonlinear buckling load,' *JSME Int. J.*, **38(3)**, 311-317, (1995).

[21] Y. Kanno, M. Ohsaki, K. Fujisawa and N. Katoh, 'Topology optimization for specified multiple linear buckling load factors by using semidefinite programming,' *Proc. 1st Int. Conf. on Struct. Stability and Dynamics (ICSSD 2000)*, pp. 267-272, (2000).

[22] K. J. Bathe, E. Ramm and E. J. Wilson, Finite element formulations for large deformation dynamic analysis, *Int. J. Num. Meth. Engng*, **9**, 353-386, (1974).

[23] K. M. Heal, M. L. Hansen and K. M. Rickard, Maple V Programming Guide, Springer, 1998.

[24] *DOT User's Manual, Ver. 4.20.*, Vanderplaats Research & Development, Inc., Colorado Spring, 1995.

Chapter 5

Heuristic methods for optimization of spatial frames.

5.1 Introduction.

In the process of architectural design, the cross-sectional properties are selected from lists or catalogs of the standard sections. Therefore, the optimization problems are formulated as combinatorial optimization problem that is generally classified as (mixed) integer programming problem.

It is very easy to solve a combinatorial optimization problem if the number of variables is small. However, the computational cost increases as an exponential function of the problem size, and it is not possible to solve a practical problem with a practically admissible computational time. If the upper and lower bounds of the objective values can be easily found, the branch-and-bound method can be used to find the globally optimal solution. However, for the structural optimization problem, the relaxed nonlinear programming problems are non-convex for which the global optimality is not guaranteed.

Recently, with the rapid development of computer hardware and software technologies, we can carry out structural analysis many times to obtain optimal solutions. Furthermore, in the practical design process, it may be enough to obtain an approximate optimal design.

Heuristic approaches have been developed to obtain approximate optimal solutions within reasonable computation time, although there is no theoretical proof of convergence. The most popular approach is the genetic algorithm (GA), which is a multi-point method that has many solutions at each iterative step. Since computational cost at each analysis is not very small, multi-point may not be appropriate for optimization of large structures. In this chapter, single-point heuristics such as greedy method, simulated annealing, taboo search, are applied to optimal design of a spatial frame, and their performances are compared.

5.2 Structural optimization with discrete variables.

Suppose a list of standard sections is given, and let the cross-sectional properties of the jth section are denoted by (A_j^0, I_j^0, Z_j^0), where A_j^0 is the cross-sectional area, I_j^0 is the second moment of area, and Z_j^0 is the sectional coefficient. $J_i = j$ $(i = 1, 2, \ldots, m)$ indicates that jth section is assigned to the ith member, where m is the number of members; i.e. the mechanical properties of the frame is defined by the integer vector $\mathbf{J} = \{J_i\}$. In the following, the components of a vector are indicated by subscripts.

The constraints on the response displacements and stresses against static loads are given as

$$g_j(\mathbf{J}) \leq 0, \quad (j = 1, 2, \ldots, n) \tag{5.1}$$

where g_j is a function of $\mathbf{J}$, and n is the number of constraints.

We consider inequality constraints only, because the constraints given by building codes are formulated as inequality. The objective function such as total structural volume is also a function of $\mathbf{J}$ which is written as $V(\mathbf{J})$. Hence the optimization problem is formulated as

$$\begin{aligned} &\text{minimize} && V(\mathbf{J}) && (5.2)\\ &\text{subject to} && g_j(\mathbf{J}) \leq 0, \quad (j = 1, 2, \ldots, n) && (5.3)\\ & && J_i \in \{1, 2, \ldots, r\}, \quad (i = 1, 2, \ldots, m) && (5.4) \end{aligned}$$

where r is the number of standard cross-sections which is same for all members, for brevity.

5.3 Overview of heuristic methods.

Heuristics are based on local search [1] which consecutively moves to a neighborhood solution if it improves (decrease for a minimization problem) the value of the objective function, where the neighborhood solutions are generated by modifying the value of one or several variables to neighboring values. Since it is not always possible to find an optimal solution by simple local searches, heuristic approaches have been proposed to improve the convergence properties.

The basic algorithm of a single-point heuristic approach can be written as

Basic algorithm of heuristic approach

Step 1 Assign initial solution.

Step 2 Generate neighborhood solutions, and select a solution based on a local search algorithm.

Step 3 Update the solution in accordance with the algorithm.

Step 4 Go to Step 2 if not converged.

For the initial solution, we can assign either specified or randomly generated values. An optimal solution by another approach can be modified to be used as the initial solution; e.g. the nearest discrete solution from the optimal solution with continuous variables can be used. The neighborhood solutions are the set of solutions that can be reached from the current solution by the specified operation; e.g. the rank of the cross-section of a randomly selected member can be increased or decreased to obtain a neighborhood solution.

Heuristic approaches can be classified to deterministic and probabilistic approaches. The most simple deterministic approach is the *greedy method* described as

Greedy method

Step 1 Assign an initial solution that does not satisfy the constraints; e.g. choose the smallest value for all variables for the case where the constraint functions $g_j(\mathbf{J})$ are decreasing functions of $\mathbf{J}$.

Step 2 Move to a neighborhood solution which most efficiently improves the objective function and constraints.

Step 3 Go to Step 2 if one of the constraints is not satisfied.

The reverse approach that starts from a solution satisfying all the constraints and reduces the objective value consecutively is called *stingy method* which is described as

Stingy method

Step 1 Assign an initial solution that satisfies all the constraints; e.g. choose the largest value for all variables for the case where the constraint functions $g_j(\mathbf{J})$ are decreasing functions of $\mathbf{J}$.

Step 2 Move to a neighborhood solution which most efficiently reduces the objective function.

Step 3 Go to Step 2 if all the constraints are satisfied.

The convergence property to the global optimal solution may be enhanced if several solutions are searched before moving to a neighborhood solution, However, in this case a so called *cycling* can occur where two neighboring solutions are chosen iteratively. The taboo search has been developed to prevent cycling. In the taboo search, the solutions that have been already searched are included in the taboo list of prohibited solutions. A neighborhood solution that does not improve the objective function can also be selected to improve the ability of reaching the global optimal solution.

In the case where inequality constraints are assigned, the following penalty function is used to evaluate the solution:

$$V^*(\mathbf{J}) = V(\mathbf{J}) + \sum_{j=1}^{n} \alpha_j [\max(g_j(\mathbf{J}), 0)]^2 \tag{5.5}$$

where α_j is a penalty coefficient, and no penalty is given if $g_j \leq 0$ and the constraint is satisfied.

The algorithm of taboo search is summarized as

Taboo search

Step 1 Assign initial solution and initialize the taboo list.

Step 2 Generate neighborhood solutions and move to the best solution among them that is not included in the taboo list.

Step 3 Add the solution to the taboo list.

Step 4 Remove the oldest solution in the taboo list if the length of the list exceeds the specified value.

Step 5 Go to Step 2 if the termination condition is not satisfied.

The simplest probabilistic approach is the random search which works as

Random search

Step 1 Randomly set the initial solution.

Step 2 Move to the randomly generated neighborhood solution.

Step 3 Go to Step 2 if the termination condition is not satisfied.

Although the random search is not efficient in view of convergence to the global optimal solution, it is simple and easy to implement.

The simulated annealing (SA) has been developed to prevent converging to local optimal solution by allowing the move to a solution that does not improve the objective function, where the probability of accepting such a solution is defined by the amount of increase (for minimization problem) of the objective function. The term *simulated annealing* comes from the fact that it simulates the behavior of the metals in annealing process. The basic algorithm is as follows:

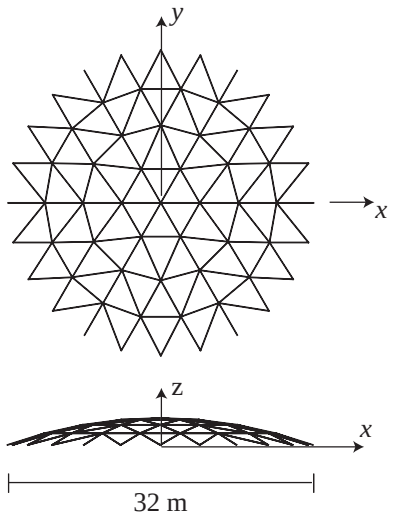

Fig. 5.1: A single-layer spatial frame.

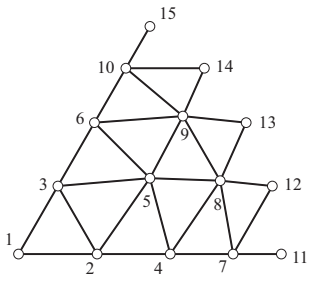

Fig. 5.2: Node numbers.

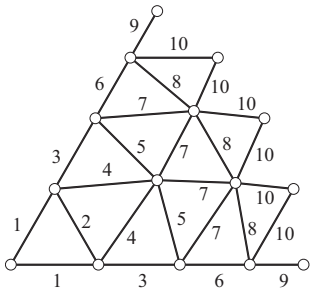

Fig. 5.3: Member numbers.

Simulated annealing

Step 1 Randomly generate the initial solution, and set the temperature parameter.

Step 2 Randomly generate a neighborhood solutions.

Step 3 Move to the neighborhood solution if it improves the objective value. If it does not improve, accept it by the probability defined by the increase (for minimization problem) of the objective value.

Step 4 Decrease the temperature parameter.

Step 5 Go to Step 2 if the termination condition is not satisfied.

5.4 Optimization of single-layer spatial frame.

Consider a 132-bar single-layer spatial frame as shown in Fig. 5.1 subjected to static loads, where the all nodes are on a sphere. The open angle is 20 degree, and the span length is 32 m. The members in the longitudinal direction have the same length. The members are rigidly jointed at the nodes, and pin jointed at the supports. The node numbers and nodal coordinates are as shown in Fig. 5.2 and Table 5.1, respectively.

Table 5.1: Nodal coordinates. (cm)

Node number	x	y	z
1	0.0	0.0	282.124
2	407.722	0.0	264.322
3	203.860	353.098	264.322
4	812.342	0.0	211.052
5	703.508	406.170	211.052
6	406.170	703.508	211.052
7	1210.778	0.0	122.722
8	1137.760	414.110	122.722
9	927.510	778.274	122.722
10	605.388	1048.564	122.722
11	1600.0	0.0	0.0
12	1545.482	414.110	0.0
13	1385.640	800.0	0.0
14	1131.370	1131.370	0.0
15	800.0	1382.640	0.0

The elastic modulus is 200 kN/mm^2, and the weight density is 7.7×10^{-5} N/mm^2. The concentrated load 40 kN is applied in the negative z-direction at each node, and self-weight is additionally considered.

The objective function to be minimized is the total structural volume, and the constraints are given for the members stresses with upper bound 50 N/mm^2. In the following, the ratio of maximum absolute value of the stresses among all members to the upper-bound stress is called *stress ratio*.

The members have cylindrical cross-sections, where the external and internal radii are denoted by R and r, respectively. For simplicity, we assume the relation between R and r as

$$r = 0.96R \tag{5.6}$$

Therefore, all the cross-sectional properties such as cross-sectional area and second moment of area are defined by R. The members are divided into ten groups as shown in Fig. 5.3, and the external radius of the members in group i is denoted by R_i. A list $\mathbf{R}^0$ is given as follows, from which R_i of each group is to be selected:

$$\mathbf{R}^0 = \{60, 120, 180, 240\} \tag{5.7}$$

where the unit of length is mm.

Optimal solution is first found by considering R_i as continuous variables. Optimization is carried out by a nonlinear programming program IDESIGN Ver. 3.5 [1], where the sequential quadratic programming (SQP) is used. The lower bound for R_i is 60 mm, and the upper bound is not given. The optimal solution is as listed in the 2nd column of Table 5.2. Note that the number of analyses is 1233, which is very large, because the finite difference approach is used for design sensitivity analysis.

The nearest value of R_i from the continuous solution is selected from the list $\mathbf{R}^0$. The rank of R_i corresponding to the maximum stress ratio is increased consecutively. Result of this greedy method (type 1) is listed in the 3rd column of Table 5.2, where the number of analyses is 4 for the greedy method added by 1233 for SQP to result in $1233 + 4 = 1237$.

To confirm the accuracy of the heuristic methods, the global optimal solution has been found by enumerating all the solutions. The result is listed in the 4th column of Table 5.2. Note that the simple greedy method (type 1) could reach a good approximate solution.

Next we consider a greedy method (type 2) starting from $R_i = 60$ mm for all the members. The result is listed in the 5th column of Table 5.2. On the other hand, if we use the stingy method

Table 5.2: Optimal external radius (Part 1)

Group	Continuous	Greedy type 1	Enumeration	Greedy type 2	Stingy
1	184.2	4	4	4	4
2	60.0	1	1	1	1
3	156.3	3	3	4	3
4	116.2	2	2	1	2
5	109.2	2	2	3	3
6	153.0	3	3	4	4
7	126.9	3	3	3	3
8	117.9	2	2	1	1
9	60.0	2	1	2	2
10	144.5	3	3	3	3
V (m^3)	2.504	3.831	3.766	3.996	4.005
Maximum stress ratio	1.000	0.9957	0.9746	0.9409	0.8961
No. of analyses	1233	1237	489331	16	14

Table 5.3: Optimal external radius (Part 2)

Member group	SA	Random search	Taboo search	Enumeration near continuous solution	Greedy type 3
1	4	4	4	4	4
2	2	1	1	1	1
3	3	3	3	3	4
4	2	2	2	2	2
5	2	2	3	2	3
6	3	3	3	3	4
7	3	3	2	3	3
8	2	2	3	2	1
9	1	2	2	1	2
10	3	3	3	3	3
V (m^3)	3.831	3.766	3.870	3.766	4.157
Maximum stress ratio	0.9980	0.9746	0.8961	0.8441	0.9746
No. of analyses	2000	2000	100	2256	1244

starting from the initial solution $R_i \equiv 240$ mm, the result is as shown in the 6th column of Table 5.2. In this case, the stingy method reached a better solution than the greedy method (type 2). The number of analyses is very small for both methods.

The result by SA is listed in the 2nd column of Table 5.3, where the penalty parameter is 10^{11} which is same for all the examples below. The initial value of the temperature parameter is 1, which is multiplied by 0.99 at each iterative step. We tried 10 cases with 200 steps for each case. Therefore, the number of analyses is 2000. The result by a random search is listed in the 3rd column of Table 5.3, where the number of analyses is also 2000. Note that the random search has better performance than SA for this example.

The result by a taboo search is as shown in the 4th column of Table 5.3, where the length of the taboo list is 50, and the number of the neighborhood solutions is 20 for general case. A good approximate solution has been found by the taboo search.

The 5th column of Table 5.3 shows the result of enumeration in the neighborhood of the continuous solution. In this example, there exists a global optimal solution in the neighborhood of the continuous solution.

Finally a greedy method (type 3) has been tried starting from the value of R_i in the list that does not exceed the continuous solution. The result is listed in the 6th column of Table 5.3. In this

Table 5.4: Comparison of performances of the heuristic approaches

	$R = 60$	$R = 58$	$R = 56$	$R = 54$	$R = 52$	$R = 50$
Greedy (type 1)	3.831	3.831	3.836	3.567	3.557	3.186
Enumeration	<u>3.766</u>	<u>3.682</u>	<u>3.565</u>	<u>3.314</u>	<u>3.259</u>	<u>3.092</u>
Greedy (type 2)	3.996	4.026	3.754	3.709	4.249	4.434
Stingy	4.005	3.743	3.621	4.634	4.297	5.092
SA	3.831	<u>3.682</u>	3.587	<u>3.514</u>	<u>3.259</u>	3.137
Random search	<u>3.766</u>	<u>3.682</u>	3.586	<u>3.314</u>	3.273	3.102
Taboo search	3.996	<u>3.682</u>	<u>3.565</u>	<u>3.314</u>	<u>3.259</u>	<u>3.092</u>
Enumeration near continuous solution	<u>3.766</u>	3.728	3.709	3.721	3.450	3.102
Greedy (type 3)	4.157	3.831	3.836	3.567	3.557	4.037

case, no good solution has been found by this approach.

The optimization results presented above, however, strongly depend on the geometry of the structure, available values of R_i, load level, etc. In the following we parametrically vary the available values of R_i, and compare the performances of the heuristic approaches.

Let $\bar{R}$ denote the unit value of available R_i, and define the list $\mathbf{R}^0$ as

$$\mathbf{R}^0 = \{\bar{R}, 2\bar{R}, 3\bar{R}, 4\bar{R}\} \tag{5.8}$$

The optimal objective values for $\bar{R} = 60, 58, 56, 54, 52, 50$ by each method are listed in Table 5.4, where the underline indicates the global optimal solution. The following observation can be obtained from Table 5.4:

1. SA and random search can reach global solution or a good approximate solution.
2. Greedy methods and stingy method may find a solution that has very large objective value.
3. It often happens that the global solution does not exist in the neighborhood of the continuous solution.

5.5 Conclusions

The basic concepts of heuristic methods have been presented, and a variety of methods have been applied to the optimization problem under stress constraints of a spatial frame.

We limited the scope within one-point search methods such as SA and greedy method. Application of the genetic algorithm, which is the most popular multi-point search method, may be found in many monographs and papers.

From the numerical experiences, the possibility of obtaining the global optimal solution is very large, if several simple approaches are tried.

References

[1] E. Aarts and J. K. Lenstra (Eds.), Local Search in Combinatorial Optimization, John Wiley & Sons, 1997.

[2] E. E. Goldberg, Genetic Algorithms in Search, Optimization, and Machine Learning, Addison-Wesley, 1989.

[3] E. Aarts and J. Korst, Simulated Annealing and Boltzmann Machine, John Wiley & Sons, 1989.

[4] J. S. Arora and C. H. Tseng, IDESIGN User's Manual, Ver. 3.5, Optimal Design Laboratory, The University of Iowa, 1987.

Appendix A

Overview of Structural Optimization

A.1 What is structural optimization?

The definition, roles, and classification of structural optimization are summarized in this chapter. The whole process of structural design may be regarded as that of seeking the best set of design variables under given design requirements, where the variables that can be determined by the designers are called *design variables* that include the cross-sectional areas, locations of members and nodes of frames and trusses. The basic strategy of structural design may be simply stated as

- Find his/her best solution by modifying the design variables based on the experience and trial-and-error process.

However, the following questions may arise:

- How the *best solution* defines?
- How can we modify the design variables if the solution is not preferable?

Optimization can answer these questions.

The structural optimization problem is regarded as an application of optimization problems to the field of structural design[1–3]. The optimization problems have been mainly developed in applied mathematics and management science where the related fields are called operations research (OR).

In the traditional design process, arbitrary initial values are given for the design variables, and the response analysis is carried out. The variables are then modified if the design requirements are not satisfied. In this process, however, the variables are modified based on the experience and intuition of the designers and engineers; i.e. there is no general criterion for design modification. Furthermore, the design process is terminated if all the requirements are satisfied, and no effort is done for finding better solutions.

On the other hand, structural optimization provides us with the following benefits:

- The solution can be found automatically and efficiently satisfying all the constraints on the responses such as stresses and displacements, and simultaneously minimizing the objective function such as total structural volume.
- The optimization tool helps decision making of the designer; i.e. it is not an automatic design tool that has negative impressions to the structural engineers and designers.
- The designers can spend more time for the jobs of higher level if optimization tools are effectively used for decision making.
- Even if the optimal solution cannot be used directly in design practice, the solution gives insight to the better design.

A.2 General formulation of optimization problem.

The optimization problem can be formally formulated as

Cost minimization problem:

$$\begin{aligned} &\text{minimize} && \textit{objective function (cost, weight, volume)} \\ &\text{subject to} && \textit{constraints on mechanical performances} \end{aligned}$$

where *subject to* means *under constraints on*, and the mechanical performance includes member stresses, nodal displacements, etc. The minimization problem can be alternatively written as

$$\textit{objective function} \rightarrow \text{minimize}$$

The constraints are determined from building codes. The total structural volume (or weight) is usually given as the objective function, because

- Generally reduction of the weight leads to less cost, especially for spatial structures where the self-weight has the large portion of the design loads.
- Irrespective of the definition of the objective function, it is important that a solution satisfying all the constraints, called *feasible solution*, is obtained after optimization.

If the concept of minimum weight is not acceptable, the following formulation will be better:

Performance maximization problem:

$$\begin{aligned} &\text{maximize} && \textit{mechanical performance} \\ &\text{subjectto} && \textit{upper bound for cost (weight, volume)} \end{aligned}$$

Consider, e.g., the problem of minimizing the structural volume under constraints on stresses and displacements against static loads. The design variables are the cross-sectional areas of the members. Let $\boldsymbol{\sigma}$ and $\mathbf{U}$ denote the vectors of member stresses and nodal displacements. The cross-sectional area and the length of the ith member is denoted by A_i and L_i, respectively. The optimization problem is formulated as

Truss optimization problem:

$$\begin{aligned} &\text{minimize} && \sum_{i=1}^{m} A_i L_i \\ &\text{subject to} && \boldsymbol{\sigma}^{\mathrm{L}} \leq \boldsymbol{\sigma} \leq \boldsymbol{\sigma}^{\mathrm{U}} \\ & && \mathbf{U}^{\mathrm{L}} \leq \mathbf{U} \leq \mathbf{U}^{\mathrm{U}} \\ & && \mathbf{A}^{\mathrm{L}} \leq \mathbf{A} \leq \mathbf{A}^{\mathrm{U}} \end{aligned}$$

where m is the number of members, and the upper and lower bounds are denoted by the superscripts U and L, respectively.

If $\mathbf{A}$ is continuous, then the truss optimization problem is a nonlinear programming problem. On the other hand, if the cross-sectional area is selected from a list or a catalog, then the problem is a combinatorial optimization problem that can be solved by mixed integer programming approaches or heuristics such as genetic algorithms and simulated annealing [4, 5].

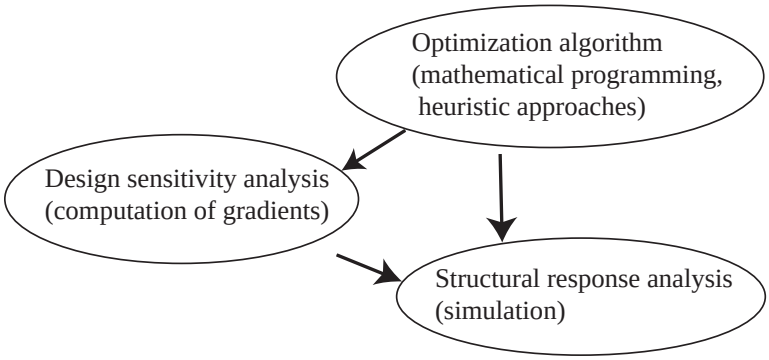

Fig. A.1: Relation among optimization, response analysis and design sensitivity analysis.

A.3 What is needed for structural optimization?

The solution methods of structural optimization may be divided to *gradient-based mathematical programming approach* and *heuristics*. In the latter approach, the optimal solutions can be found if analysis can be done many times. In the former approach, design sensitivity analysis to compute the gradients of objective and constraint functions with respect to the design variables should be carried out. Analysis and sensitivity analysis are consecutively done and the design variables are modified in accordance with the optimization algorithm as illustrated in Fig. A.1.

There are many freewares for mathematical programming that can be found in websites, e.g.

- NEOS(Network-Enabled Optimization System): http://www-neos.mcs.anl.gov/
- Netlib: http://www.netlib.org/
- GAMS: http://www.gams.com/

Therefore, the structural engineers just have to use the software packages or libraries to obtain optimal solutions. However, fundamental knowledge of optimization is important because

- If you do not know the class of the problem to be solved, you cannot find an appropriate software.
- If you need to modify the input parameters for optimization, you should know the meaning of the parameter.
- If you do not have any expertise, you just abandon optimization when no solution could be found by simply setting the input parameter as default value.

A.4 What can we get from optimization?

In view of code-based design, effectiveness of using optimization approach may be summarized as

- Solution satisfying all the constraints are obtained, if the problem is appropriately formulated.
- Optimization is very helpful for special structures, such as space frames, where even a designer with enough experience cannot find a feasible design.
- If we start from a solution found by an expert, the solution cannot be worse after optimization, and usually a better solution can be found.

Furthermore, in view of decision making,

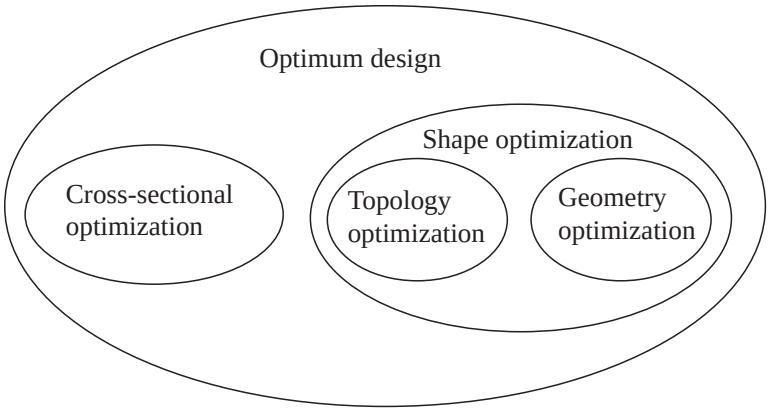

Fig. A.2: Classification of structural optimization based on design variables.

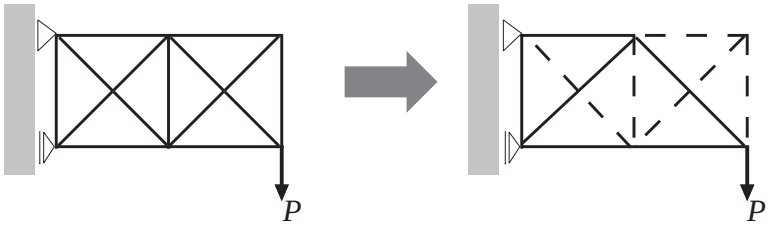

Fig. A.3: Topology optimization.

- The trade-off relation between the cost and performance, as well as the process of decision making, can be made clear, if optimization is carried out several times by modifying the input parameters such as the cost coefficients and upper bound of responses.

The most positive way of using optimization may be

- Find new structural system and shape by optimization.
- Realize innovative structure that cannot be found without optimization.

A.5 Classification of structural optimization.

There are several approach to classification of structural optimization problems. One of the traditional classification for trusses and frames is as shown in Fig. A.2. The cross-sectional properties are optimized in *cross-sectional optimization* (*sizing optimization*). The *shape optimization* includes *geometry optimization* (*configuration optimization*) and *topology optimization* [6], where the nodal locations and member connectivity are optimized, respectively.

A process of topology optimization under stress constraints is illustrated in Fig. A.3, where the dotted lines indicate the removed members after optimization. This approach of removing unnecessary members from the highly connected initial structure is called *ground structure approach*.

Fig. A.4 illustrates the process of geometry optimization, where the gray rectangles indicate feasible regions of the nodes. In geometry optimization the feasible regions of the nodes are restricted so that the topology of the structure does not change. Therefore, simultaneous optimization of topology and geometry is very difficult [7].

In the following, effectiveness of topology optimization and geometry optimization is demonstrated using a simple beam supported by a cable as shown in Fig. A.5. The objective is to design

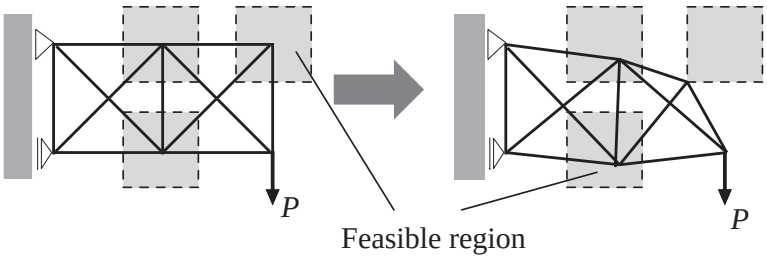

Fig. A.4: Geometry optimization.

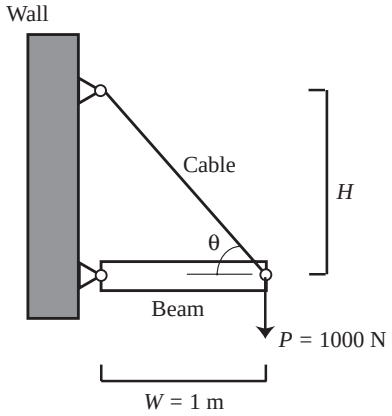

Fig. A.5: Coat-hanger problem.

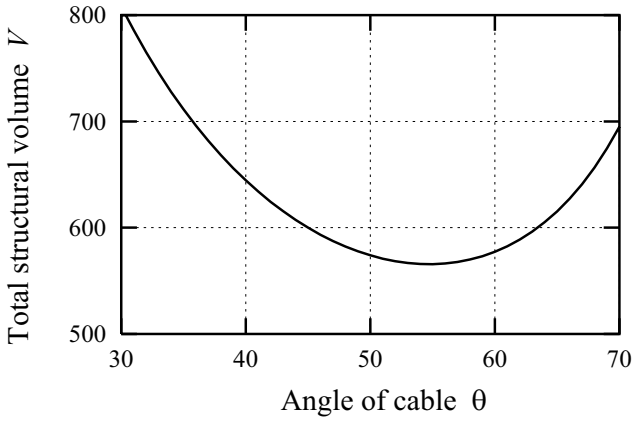

Fig. A.6: Relation between the angle of the cable and the optimal structural volume.

a frame to hang a object of 1000 N at a place 1 m from the wall. This type of problem is called *coat-hanger problem*.

Constraints are given for the stresses, and the total structural volume is to be minimized. Let θ denote the angle between the cable and the beam. Then the length of the cable is $1/\cos\theta$ m, and the absolute values of the axial forces of the beam and the cable are $1000/\tan\theta$ N and $1000/\sin\theta$ N, respectively.

If we decrease the cross-sectional areas, then the structural volume decreases, but the stresses increase. Therefore, there exist optimal cross-sectional areas under stress constraints. For the upper-bound stress 50 N/mm^2, the stresses are equal to the upper bound, and the structural volume V has the minimum value $200/\tan\theta + 200/(\sin\theta\cos\theta)$ mm^3, when the cross-sectional areas of the cable

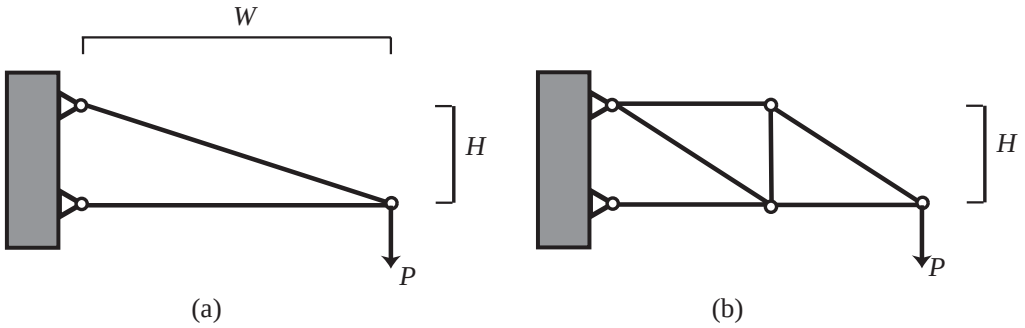

Fig. A.7: Example of topology for the case where H/W is small.

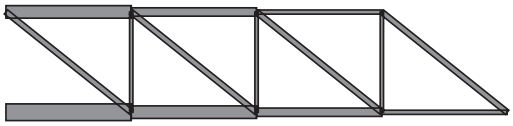

Fig. A.8: Optimal cross-sectional areas for four units.

Table A.1: Relation between the number of units and the optimal structural volume.

Number of units	2	3	4	5	6
Optimal structural volume m^3	16.20	15.33	15.30	15.60	16.07

and the beam are $200/\tan\theta$ mm^2 and $200/\sin\theta$ mm^2, respectively.

If we can modify θ in addition to the cross-sectional areas; i.e. if we consider shape optimization, the relation between θ and the optimal structural volume is as shown in Fig. A.6. We can see from Fig. A.6 that V takes the minimum at $\theta \simeq 55°$.

However, in a practical situation, θ cannot be equal to 55° due to the restriction of the height of the ceiling. Obviously, if height H is small, the configuration as Fig. A.7(a) is not recommended, and a frame as Fig. A.7(b) will be better. Therefore, we next consider a truss for hanging an object. Since the truss in Fig. A.7(b) is statically determinate, an optimal design can be obtained by assigning the cross-sectional areas so that the absolute values of the stresses of all members are equal to the upper bounds.

Optimal solutions have been found for the number of units 2, 3, 4, 5 and 6, where $H/W = 0.2$. The relation between the number of units and the optimal structural volume is as listed in Table A.1. It is observed from Table A.1 that the structural volume takes minimum when the number of units is 4, and the optimal cross-sectional areas are as shown in Fig. A.8, where the width of each member is proportional to its cross-sectional area. This way, the objective values can be further reduced by optimizing the topology.

References

[1] J. S. Arora, Introduction to Optimum Design, 2nd ed., Academic Press, 2004.

[2] R. T. Haftka, Z. Gürdal and M. P. Kamat, Elements of Structural Optimization, Kluwer Academic Publishers, 1990.

[3] D. G. Luenberger, Linear and Nonlinear Programming, 2nd ed., Kluwer Academic Publisher, 2003.

[4] E. E. Goldberg, Genetic Algorithms in Search, Optimization, and Machine Learning, Addison-Wesley, 1989.

[5] E. Aarts and J. Korst, Simulated Annealing and Boltzmann Machine, John Wiley & Sons, 1989.

[6] M. P. Bendsøe and O. Sigmund, Topology Optimization: Theory, Methods and Applications, Springer, 2003.

[7] M. Ohsaki, Simultaneous optimization of topology and geometry of a regular plane truss, Comput. & Struct., Vol. 66(1), pp. 69-77, 1997.